

The CoQ oxidoreductase FSP1 acts parallel to GPX4 to inhibit ferroptosis

<https://doi.org/10.1038/s41586-019-1705-2>

Received: 25 February 2019

Accepted: 1 October 2019

Published online: 21 October 2019

Kirill Bersuker¹, Joseph M. Hendricks¹, Zhipeng Li¹, Leslie Magtanong², Breanna Ford^{1,3,4}, Peter H. Tang⁵, Melissa A. Roberts¹, Bingqi Tong³, Thomas J. Maimone³, Roberto Zoncu⁴, Michael C. Bassik⁶, Daniel K. Nomura^{1,3,4}, Scott J. Dixon² & James A. Olzmann^{1,7*}

Ferroptosis is a form of regulated cell death that is caused by the iron-dependent peroxidation of lipids^{1,2}. The glutathione-dependent lipid hydroperoxidase glutathione peroxidase 4 (GPX4) prevents ferroptosis by converting lipid hydroperoxides into non-toxic lipid alcohols^{3,4}. Ferroptosis has previously been implicated in the cell death that underlies several degenerative conditions², and induction of ferroptosis by the inhibition of GPX4 has emerged as a therapeutic strategy to trigger cancer cell death⁵. However, sensitivity to GPX4 inhibitors varies greatly across cancer cell lines⁶, which suggests that additional factors govern resistance to ferroptosis. Here, using a synthetic lethal CRISPR–Cas9 screen, we identify ferroptosis suppressor protein 1 (FSP1) (previously known as apoptosis-inducing factor mitochondrial 2 (AIFM2)) as a potent ferroptosis-resistance factor. Our data indicate that myristylation recruits FSP1 to the plasma membrane where it functions as an oxidoreductase that reduces coenzyme Q₁₀ (CoQ) (also known as ubiquinone-10), which acts as a lipophilic radical-trapping antioxidant that halts the propagation of lipid peroxides. We further find that FSP1 expression positively correlates with ferroptosis resistance across hundreds of cancer cell lines, and that FSP1 mediates resistance to ferroptosis in lung cancer cells in culture and in mouse tumour xenografts. Thus, our data identify FSP1 as a key component of a non-mitochondrial CoQ antioxidant system that acts in parallel to the canonical glutathione-based GPX4 pathway. These findings define a ferroptosis suppression pathway and indicate that pharmacological inhibition of FSP1 may provide an effective strategy to sensitize cancer cells to ferroptosis-inducing chemotherapeutic agents.

GPX4 is considered to be the primary enzyme that prevents ferroptosis². The resistance of some cancer cell lines to GPX4 inhibitors⁶ led us to search for additional protective pathways. To identify ferroptosis-resistance genes, we performed a synthetic lethal CRISPR–Cas9 screen using a sublibrary of single-guide RNAs (sgRNAs) targeting genes related to apoptosis and cancer in U-2 OS osteosarcoma cells that were treated with the GPX4 inhibitor 1S,3R-RSL3 (hereafter, RSL3) (Fig. 1a). This screen revealed a substantial dis-enrichment of sgRNAs targeting *FSP1* (currently known as *AIFM2*) in the cells treated with RSL3 (Fig. 1b, c, Extended Data Fig. 1a, Supplementary Table 1), which indicates that deletion of the *FSP1* gene is lethal in combination with RSL3 treatment. FSP1 was originally named AIFM2 on the basis of its homology with apoptosis-inducing factor (AIF or AIFM1), a mitochondrial pro-apoptotic protein^{7,8}. However, as we report here, FSP1 lacks the N-terminal mitochondrial targeting sequence in AIF, does not localize to mitochondria and does not promote apoptosis. We rename AIFM2 as FSP1 to reflect its cellular role, as described in this study.

FSP1 is a potent ferroptosis suppressor

Quantification of cell viability using time-lapse microscopy revealed a considerable increase in the sensitivity of FSP1 knockout (FSP1^{KO}) cell lines to RSL3 (Fig. 1d–f, Extended Data Fig. 1b, Supplementary Table 2), which was rescued by expression of untagged FSP1 (Extended Data Fig. 1c,d). In contrast to previous reports^{7,8}, the overexpression of FSP1 did not induce apoptosis (Extended Data Fig. 1e, f) and activation of p53 did not increase FSP1 expression (Extended Data Fig. 1g). FSP1^{KO} cells displayed increased sensitivity to additional ferroptosis inducers, including the GPX4 inhibitor ML162 and the system x_c⁻ inhibitor erastin2 (ref. 9) (Extended Data Fig. 1h), but not to the complex I inhibitor rotenone or hydrogen peroxide (Extended Data Fig. 1i–l). The viability of RSL3-treated FSP1^{KO} cells was rescued by the iron chelator deferoxamine (DFO) and by the radical-trapping antioxidants ferrostatin-1 (Fer1) and idebenone (Fig. 1g), but not by inhibitors of apoptosis (ZVAD(OMe)-FMK) or necroptosis (necrostatin-1) (Extended Data Fig. 1m). Knockout of long-chain acyl-CoA synthetase 4 (ACSL4) in

¹Department of Nutritional Sciences and Toxicology, University of California, Berkeley, Berkeley, CA, USA. ²Department of Biology, Stanford University, Stanford, CA, USA. ³Department of Chemistry, University of California, Berkeley, Berkeley, CA, USA. ⁴Department of Molecular and Cell Biology, University of California, Berkeley, Berkeley, CA, USA. ⁵Department of Pathology and Laboratory Medicine, Cincinnati Children's Hospital Medical Center and University of Cincinnati College of Medicine, Cincinnati, OH, USA. ⁶Department of Genetics and Stanford University Chemistry, Engineering and Medicine for Human Health (ChEM-H), Stanford University School of Medicine, Stanford, CA, USA. ⁷Chan Zuckerberg Biohub, San Francisco, CA, USA.
*e-mail: olzmann@berkeley.edu

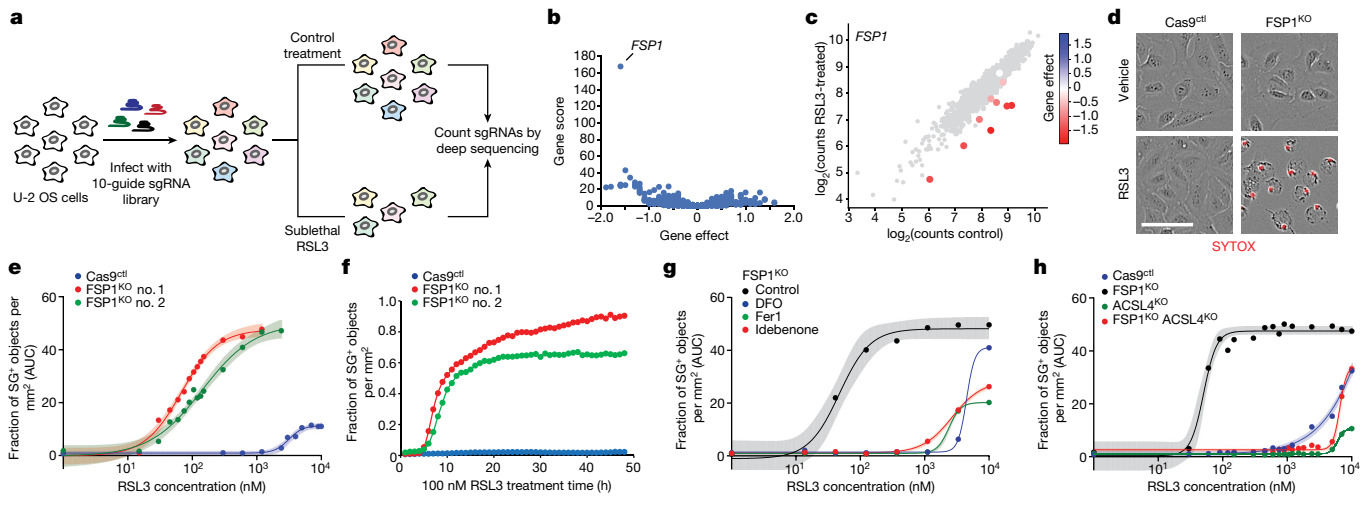


Fig. 1 | A synthetic lethal CRISPR–Cas9 screen identifies FSP1 as a ferroptosis resistance factor. **a**, Schematic of the CRISPR–Cas9 screening strategy. **b**, Gene effect and gene score calculated for individual genes analysed in the CRISPR–Cas9 screen. **c**, Cloud plot indicating count numbers corresponding to *FSP1* (colour scale) and control (grey) sgRNAs. The gene effect of individual sgRNAs targeting *FSP1* is indicated by the heat map. **d**, Live-cell imaging of control ($\text{Cas9}^{\text{ctrl}}$) and *FSP1*^{KO} cells incubated with SYTOX Green (SG*) and treated with 100 nM RSL3 for 48 h. Scale bar, 75 μm . **e**, Dose response of RSL3-induced cell death of control and *FSP1*^{KO} cells. AUC, area under the curve. **f**, Time-lapse

cell death analysis of cells treated with 100 nM RSL3 over 48 h. **g**, Dose response of RSL3-induced cell death in the presence of inhibitors of ferroptosis (Fer1, 1 μM ; DFO, 100 μM ; and idebenone, 10 μM). **h**, Dose response analysis of RSL3-induced cell death of the indicated cell lines. The *ACSL4*^{KO} and *ACSL4*^{KO} *FSP1*^{KO} lines shown were generated using *ACSL4* sgRNA no. 1. In **e**, **g**, **h**, shading indicates 95% confidence intervals for the fitted curves and each data point is the average of three technical replicates. Panels are representative of two biological replicates, except for **b** and **c**, which were derived from a single screen.

FSP1^{KO} cells (*FSP1*^{KO} *ACSL4*^{KO}) restored resistance to RSL3 to an extent similar to that of knockout of *ACSL4* alone (*ACSL4*^{KO}) (Fig. 1h, Extended Data Fig. 1n), consistent with the requirement for *ACSL4*-mediated incorporation of polyunsaturated fatty acids into phospholipids for ferroptosis²⁵. Together, these findings demonstrate that *FSP1* is a strong suppressor of ferroptosis.

Plasma-membrane *FSP1* blocks ferroptosis

FSP1 contains a short N-terminal hydrophobic sequence and a canonical flavin adenine dinucleotide-dependent oxidoreductase domain (Extended Data Fig. 1o). *FSP1* has previously been detected on lipid droplets¹⁰. To further define the localization of *FSP1*, we inserted a C-terminal halogenase tag (HaloTag) into the *FSP1* genomic locus (Fig. 2a). Similar to ectopically expressed wild-type *FSP1* tagged at the C terminus with green fluorescent protein (*FSP1*(WT)–GFP) (Extended Data Fig. 2a,b), *FSP1*–HaloTag localized to the periphery of lipid droplets and to the plasma membrane (Fig. 2b, Extended Data Fig. 2c, d). *FSP1*–HaloTag did not co-localize with endoplasmic reticulum labelled with blue fluorescent protein fused to Sec61 (BFP–Sec61) or with mitochondria labelled with MitoTracker (Extended Data Fig. 2g, h), consistent with the absence of an endoplasmic reticulum or mitochondrial targeting motif in *FSP1*. We noted an N-terminal consensus sequence for myristylation (Fig. 2c), a fatty acid modification that is known to function in membrane targeting. *FSP1* myristylation was tested using a click chemistry method that enables affinity purification of myristoylated proteins (Extended Data Fig. 3a). Using this approach, endogenous *FSP1* was affinity-purified from buoyant fractions enriched in lipid droplets (Extended Data Fig. 3b) and from whole-cell lysates (Fig. 2d). The myristylation of *FSP1*(WT)–GFP was blocked by the inhibition of *N*-myristoyltransferase (NMT), mutation of the glycine-2 of *FSP1* to alanine (*FSP1*(G2A)–GFP) and treatment with the translation inhibitor emetine (Fig. 2d, Extended Data Fig. 3c). Chemical and genetic perturbations of *FSP1* myristylation blocked *FSP1* recruitment to lipid droplets (Fig. 2e, Extended Data Fig. 3d, e). Although a portion of *FSP1*(G2A)–GFP was observed in proximity to the plasma membrane by total internal reflection fluorescence (TIRF) microscopy

(Extended Data Fig. 2f), the fractionation of organelles in iodixanol (OptiPrep) gradients revealed that *FSP1*(G2A)–GFP was present at lower levels in fractions enriched in plasma membrane (Fig. 2f, g, Extended Data Fig. 2i). Together, these results indicate that the myristylation of *FSP1* mediates the recruitment of this protein to lipid droplets and the plasma membrane.

Expression of *FSP1*(WT)–GFP, but not of *FSP1*(G2A)–GFP, rescued the resistance of *FSP1*^{KO} cells to RSL3 (Fig. 2h, Extended Data Fig. 3f), which indicates that *FSP1* must be myristoylated to suppress ferroptosis. We generated fusion proteins that selectively target *FSP1*(G2A)–GFP to the endoplasmic reticulum (amino acids 100–134 of cytochrome *b5*; *Cb5*), the outer mitochondrial membrane (TOM20 signal sequence, TOM20(SS)), lipid droplets (PLIN2) and the plasma membrane (first 11 amino acids of LYN kinase; LYN11) (Extended Data Fig. 4a, b). Only the expression of *FSP1* targeted to the plasma membrane (LYN11–*FSP1*(G2A)–GFP) was sufficient to restore ferroptosis resistance in *FSP1*^{KO} cells (Fig. 2i, Extended Data Fig. 4c). By contrast, expression of *FSP1*(G2A)–GFP targeted to the endoplasmic reticulum, mitochondria or lipid droplets had no effect (Fig. 2j). Consistent with previous results in HT1080 cells¹¹, the depletion of lipid droplets using inhibitors of the diacylglycerol acyltransferase enzymes (DGAT1 and DGAT2) did not affect ferroptosis sensitivity (Extended Data Fig. 5a–c), which provides support for the conclusion that lipid-droplet localization is not required for the *FSP1*-mediated suppression of ferroptosis. Thus, *FSP1* plasma-membrane localization is necessary and sufficient to confer ferroptosis resistance.

FSP1 reduces CoQ to suppress ferroptosis

Under basal conditions, the ratiometric fluorescent lipid peroxidation sensor BODIPY 581/591 C11 exhibited similar levels of oxidation in control and *FSP1*^{KO} cells (Fig. 3a, Extended Data Fig. 6a, b). However, a brief treatment with RSL3 strongly increased C11 oxidation in *FSP1*^{KO} cells relative to control (Fig. 3a, Extended Data Fig. 6a, b). Glutathione levels were unaffected in *FSP1*^{KO} cells (Extended Data Fig. 6c–e), indicating that deletion of *FSP1* does not inhibit system x_c^- or glutathione synthesis. *FSP1*^{KO} cells also did not exhibit higher levels of phospholipids

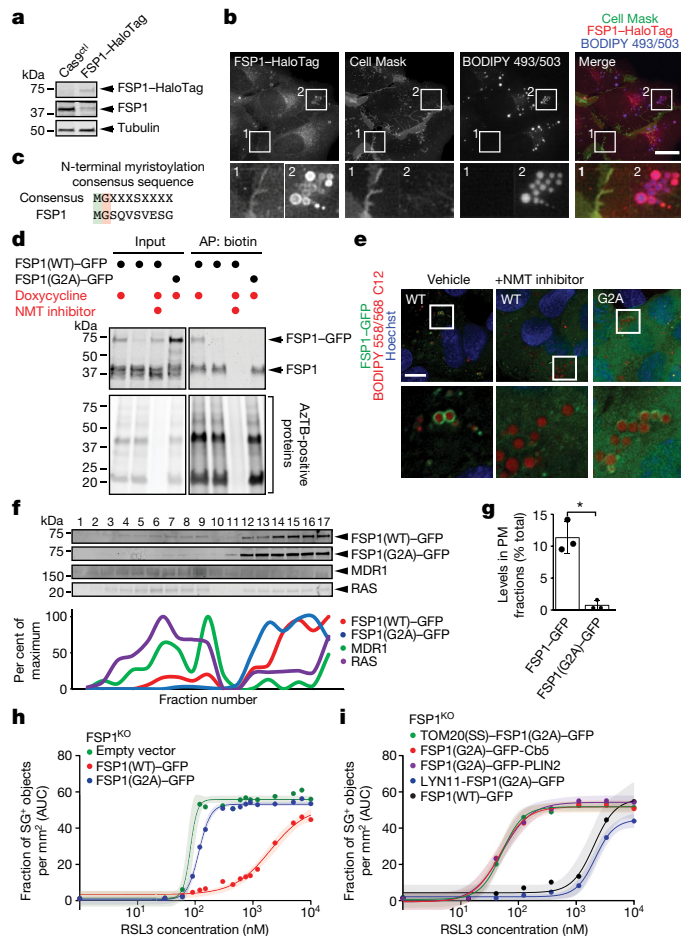


Fig. 2 | Myristoylation-dependent recruitment of FSP1 to the plasma membrane promotes ferroptosis resistance. **a**, Western blot of lysates from FSP1-HaloTag genomic knock-in cells. **b**, FSP1-HaloTag subcellular distribution by live-cell microscopy. Cells were incubated with 100 nM MJF549 to label FSP1-HaloTag, 5 μg ml⁻¹ Cell Mask to label the plasma membrane and 1 μg ml⁻¹ BODIPY 493/503 to label lipid droplets. **c**, Consensus myristoylation sequence in FSP1. **d**, Analysis of FSP1-GFP myristylation in whole-cell lysates of the indicated cell lines treated for 24 h with doxycycline to induce FSP1-GFP expression. Where indicated, 10 μM NMT inhibitor was added for 24 h to inhibit myristylation. AP, affinity purification; AzTB, TAMRA-azide-PEG-biotin. **e**, Live-cell microscopy of inducible FSP1-GFP cell lines treated with 200 μM oleate and 1 μM BODIPY 558/568 C12. Where indicated, cells were treated concurrently with 10 μM NMT inhibitor. **f**, Subcellular fractionation of organelles from cells that express FSP1-GFP, using OptiPrep gradient centrifugation. The densitometry plot shows the distribution of the indicated overexpressed and endogenous proteins. **g**, Quantification of FSP1-GFP levels in fractions 1–10 in **f**. The graph shows mean ± s.d. of $n=3$ biological replicates. *P = 0.0124 by two-tailed t-test. PM, plasma membrane. **h**, Dose response of RSL3-induced death of FSP1^{KO} cells pretreated with doxycycline for 48 h to induce expression of the indicated FSP1-GFP proteins. **i**, Dose response of RSL3-induced death of FSP1^{KO} cells that express the indicated inducible FSP1(G2A)-GFP constructs. In **h**, **i**, shading indicates 95% confidence intervals for the fitted curves and each data point is the average of three technical replicates. All panels are representative of two biological replicates. Images are representative of at least $n=10$ imaged cells. Scale bars, 10 μm.

that contain polyunsaturated fatty acids (Extended Data Fig. 6f, g, Supplementary Table 3). Levels of phospholipids containing polyunsaturated fatty acids were decreased and the corresponding lysophospholipids were increased (Extended Data Fig. 6f, g, Supplementary Table 3), a known lipidomic signature of ferroptosis that reflects the removal of oxidized polyunsaturated fatty acids from the *sn*-2 position

of phospholipids^{3,12}. These results suggest that the loss of FSP1 results in increased phospholipid oxidation even when GPX4 is functional, and that FSP1 prevents lipid peroxidation through a mechanism that is distinct from glutathione-dependent protective pathways.

FSP1 functions as an NADH-dependent CoQ oxidoreductase in vitro¹³. Reduced CoQ can act as a radical-trapping antioxidant, and idebenone—a soluble analogue of CoQ—is sufficient to suppress lipid peroxidation (Extended Data Fig. 7a) and ferroptosis¹⁴ (Fig. 1g). Previous studies have detected high levels of CoQ in non-mitochondrial compartments, including the plasma membrane^{15,16}, but the function of this molecule in these compartments remains unclear. To examine the role of FSP1 CoQ oxidoreductase activity in suppressing ferroptosis, we mutated a conserved glutamate residue (E313 in AIF or E156 in FSP1) that is required for the binding of AIF to its cofactor, flavin adenine dinucleotide (Extended Data Fig. 7b, c). Mutation of E156 in FSP1 (FSP1(E156A)-GFP) did not affect FSP1-GFP expression or localization (Extended Data Figs. 3f, 7d, e) but greatly impaired FSP1-mediated reduction of coenzyme Q₁ and resazurin in vitro (Extended Data Fig. 7f–h) and abolished the ability of FSP1-GFP to rescue the resistance of FSP1^{KO} cells to RSL3 (Fig. 3b). Consistent with these findings, the expression of FSP1(WT)-GFP, but not of FSP1(E156A)-GFP, increased the ratio of reduced-to-oxidized CoQ (Fig. 3c). Acute reduction of cellular CoQ levels by the inhibition of the CoQ biosynthesis enzyme COQ2 with 4-chlorobenzoic acid (4-CBA) strongly sensitized control cells and—to a lesser extent—FSP1^{KO} cells to RSL3-induced ferroptosis (Fig. 3d, e, Extended Data Fig. 8a). Treatment with 4-CBA also suppressed the ability of FSP1(WT)-GFP to rescue FSP1^{KO} cells (Extended Data Fig. 8b). A similar degree of sensitization to RSL3 was observed after knockout of COQ2 in control, but not in FSP1^{KO} cells (Fig. 3f, g, Extended Data Fig. 8c) and COQ2^{KO} cells exhibited increased C11 oxidation after treatment with RSL3 that was suppressed by DFO and by idebenone (Extended Data Fig. 8d, e). These data indicate that FSP1 and the CoQ synthesis machinery function in the same pathway to suppress lipid peroxidation and ferroptosis.

Deletion of NQO1, a quinone and CoQ oxidoreductase that has previously been proposed to function in ferroptosis¹⁷, did not affect sensitivity to RSL3, but cells that lack both FSP1 and NQO1 (FSP1^{KO} NQO1^{KO}) were more sensitive than FSP1^{KO} cells (Extended Data Fig. 9a–c). NQO1-GFP did not rescue ferroptosis resistance in FSP1^{KO} cells to the same extent as did FSP1-GFP (Extended Data Fig. 9d–g), even when targeted to the plasma membrane (LYN11–NQO1-GFP) (Extended Data Fig. 9h, i). These results indicate that FSP1 is unique in its ability to suppress ferroptosis through the reduction of CoQ.

FSP1 in cancer ferroptosis resistance

The Cancer Therapeutics Response Portal (CTRP) reports correlations between gene expression and drug resistance for over 800 cancer cell lines¹⁸. Data mined from the CTRP indicate that FSP1 expression positively correlates with resistance to multiple GPX4 inhibitors (RSL3, ML210 and ML162) (Fig. 4a, b, Extended Data Fig. 10a, b, Supplementary Table 4)—even more so than the system x⁻ component and erastin target SLC7A11⁹. Thus, FSP1 is a biomarker of ferroptosis resistance in many types of cancer. Consistent with the correlations observed in the CTRP, lung cancer cell lines that express low levels of FSP1 were the most sensitive to RSL3 and cell lines that express high levels of FSP1 were the most resistant (Fig. 4b, Extended Data Fig. 10c). Knockout of FSP1 in the highly resistant H460 cell line resulted in a notable, approximately 100-fold sensitization to RSL3 (Fig. 4d, Extended Data Fig. 10d, e) and overexpression of FSP1-GFP in sensitive H1703 and H446 cells increased resistance to RSL3 by about 10–20 fold (Fig. 4e, Extended Data Fig. 10f–i).

To examine the possibility that the inhibition of FSP1 could be a clinically relevant approach to sensitize tumours to ferroptosis-activating chemotherapies, we used ferroptosis-resistant H460 lung cancer cells in a preclinical tumour xenograft mouse model. Owing to the poor

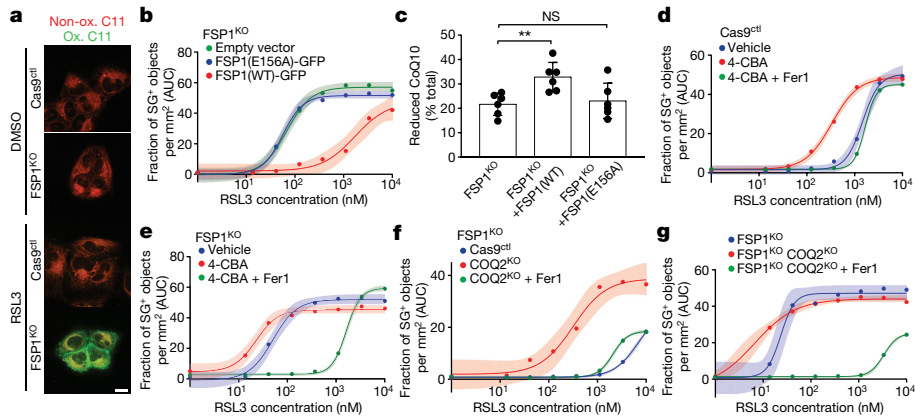


Fig. 3 | FSP1 suppresses lipid peroxidation by reducing CoQ. **a**, Control and FSP1^{KO} cells treated with 250 nM RSL3 for 75 min were labelled with BODIPY 581/591 C11 and fixed before imaging. Ox., oxidized; Non-ox., non-oxidized. Images are representative of at least 30 cells imaged for each treatment condition. Scale bar, 20 μ m. **b**, Dose response of RSL3-induced cell death of FSP1^{KO} cells that express the indicated inducible FSP1-GFP constructs. **c**, Reduced-to-oxidized CoQ ratio in FSP1^{KO} and FSP1^{KO} cells that express the indicated FSP1-GFP constructs. Data represent mean \pm s.d. of $n=6$ biological replicates. ** $P=0.0178$, NS, not significant ($P>0.99$), by one-way analysis of variance (ANOVA). **d**, **e**, Dose response of RSL3-induced death of control (**d**) and FSP1^{KO} (**e**) cells pretreated for 24 h with 3 mM 4-CBA. **f**, **g**, Dose response of RSL3-induced cell death of COQ2^{KO} (**f**) and FSP1^{KO} COQ2^{KO} (**g**) cells. In **b**, **d**–**g**, shading indicates 95% confidence intervals for the fitted curves and each data point is the average of three technical replicates. All figures are representative of two biological replicates.

bioavailability of small-molecule GPX4 inhibitors (such as RSL3), we adopted a recently developed strategy to acutely induce ferroptosis *in vivo*^{19,20} using GPX4 knockout (GPX4^{KO}) cells (Extended Data Fig. 10j). These cell lines were maintained in Fer1-containing medium to prevent the induction of ferroptosis. Fer1 washout had no effect on the viability of the GPX4^{KO} cells but resulted in the rapid death of GPX4^{KO} FSP1^{KO}

cells (Fig. 4f), consistent with our findings that FSP1 compensates for loss of GPX4 activity. Tumour xenografts were generated with GPX4^{KO} and GPX4^{KO} FSP1^{KO} H460 cell lines, and Fer1 was injected daily to allow viable tumours to develop. After tumours were established, Fer1 injections were discontinued in one set of mice to induce ferroptosis. In contrast to the GPX4^{KO} tumours (which continued to increase in size

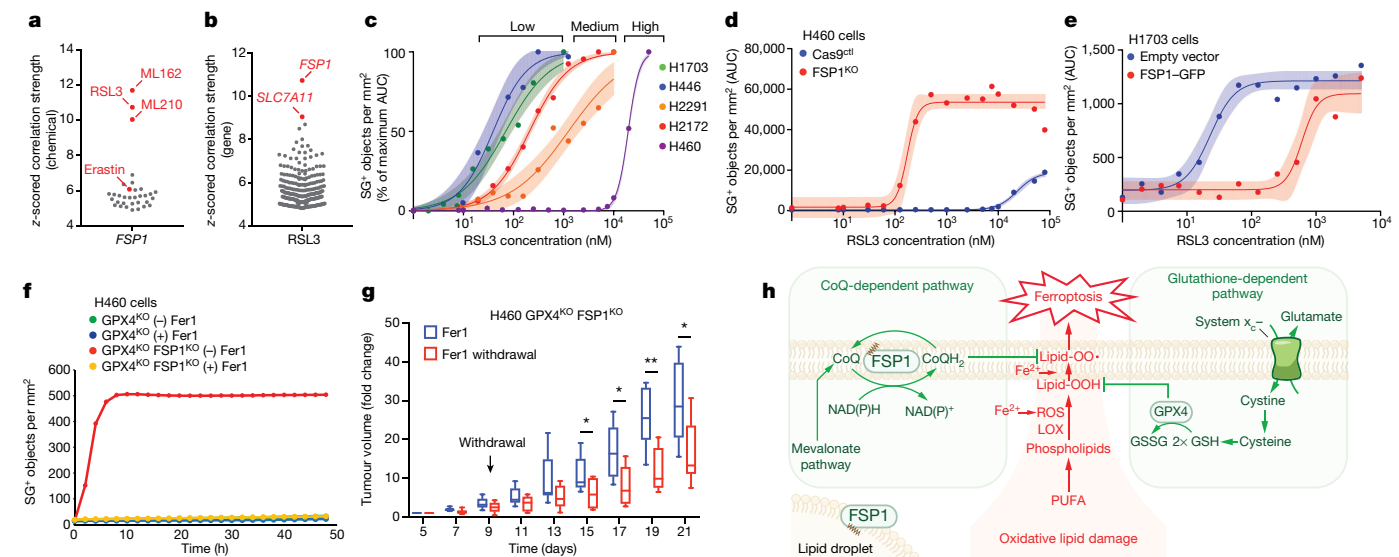


Fig. 4 | FSP1 mediates ferroptosis resistance in lung cancer. **a**, **b**, A high level of expression of FSP1 is correlated with resistance to GPX4 inhibitors in non-haematopoietic cancer cells. Plotted data were mined from the CTRP database, which contains correlation coefficients between gene expression and drug sensitivity for 907 cancer cell lines treated with 545 compounds. **a**, Correlation between FSP1 expression and resistance to individual compounds. **b**, Correlation between expression levels of individual genes and resistance to RSL3. Plotted values are z-scored Pearson's correlation coefficients. **c**, Dose response of RSL3-induced cell death of the indicated cell lines. **d**, Dose response of RSL3-induced cell death of control and FSP1^{KO} H460 cells. **e**, Dose response of RSL3-induced cell death of FSP1-GFP H1703 cells. **f**, Time-lapse analysis of cell death of GPX4^{KO} and GPX4^{KO} FSP1^{KO} H460 cells in the presence and absence of 1 μ M Fer1. **g**, GPX4^{KO} FSP1^{KO} H460 tumour xenograft cells were initiated in immune-deficient SCID mice ($n=16$). Following 5 days of daily Fer1 injections (2 mg kg⁻¹ body weight) to allow the cell lines to develop tumours, one set of mice ($n=8$) continued to receive daily Fer1 injections and a second set ($n=8$) received vehicle injections for the remaining 17 days. The distribution of fold changes in sizes of individual tumours during the treatment is shown. GPX4^{KO} FSP1^{KO} (-) Fer1, $n=7$; GPX4^{KO} FSP1^{KO} (+) Fer1, $n=8$. Box plots indicate median, 25th and 75th percentiles, and minima and maxima of the distributions. Day 15, * $P=0.0397$; day 17, * $P=0.0187$; day 18, ** $P=0.0025$; day 21, * $P=0.0327$ by two-tailed *t*-test. **h**, Model illustrating the mechanism by which FSP1 suppresses ferroptosis. In **c**–**e**, shading indicates 95% confidence intervals for the fitted curves and each data point is the average of three technical replicates. Panels **c**–**f** are representative of two biological replicates.

initiated in immune-deficient SCID mice ($n=16$). Following 5 days of daily Fer1 injections (2 mg kg⁻¹ body weight) to allow the cell lines to develop tumours, one set of mice ($n=8$) continued to receive daily Fer1 injections and a second set ($n=8$) received vehicle injections for the remaining 17 days. The distribution of fold changes in sizes of individual tumours during the treatment is shown. GPX4^{KO} FSP1^{KO} (-) Fer1, $n=7$; GPX4^{KO} FSP1^{KO} (+) Fer1, $n=8$. Box plots indicate median, 25th and 75th percentiles, and minima and maxima of the distributions. Day 15, * $P=0.0397$; day 17, * $P=0.0187$; day 18, ** $P=0.0025$; day 21, * $P=0.0327$ by two-tailed *t*-test. **h**, Model illustrating the mechanism by which FSP1 suppresses ferroptosis. In **c**–**e**, shading indicates 95% confidence intervals for the fitted curves and each data point is the average of three technical replicates. Panels **c**–**f** are representative of two biological replicates.

Article

irrespective of Fer1; Extended Data Fig. 10k), Fer1 withdrawal resulted in a significant reduction in the growth of the GPX4^{KO} FSP1^{KO} tumours (Fig. 4g). These data demonstrate that FSP1 maintains the growth of H460 lung cancer tumours *in vivo* when GPX4 is inactivated. To determine whether the growth of FSP1^{KO} tumours can be inhibited by blocking cystine import, we treated H460 cells with imidazole–ketone–erastin (IKE), a system x_c⁻ inhibitor that can induce ferroptosis *in vivo*²¹. Although U-2 OS and H460 FSP1^{KO} cells exhibited increased sensitivity to IKE in cell culture (Extended Data Fig. 10i, m), IKE did not inhibit the growth of wild-type H460 and H460 FSP1^{KO} tumour xenografts (Extended Data Fig. 10n, o). Because cells can overcome the effects of cystine depletion through the use of alternative pathways to generate glutathione²², our results underscore the need for GPX4 inhibitors that are efficacious *in vivo*.

Ferroptosis has emerged as a potential cause of cell death in degenerative diseases and as a promising strategy to induce the death of cancer cells that are resistant to other therapies^{1,2,5}. Our studies and those of a companion paper²³ identify FSP1 as a potent ferroptosis suppressor that operates in parallel to the canonical glutathione-dependent GPX4 pathway. FSP1^{KO} mice are viable and display no obvious mutant phenotypes²⁴, consistent with the compensatory suppression of lipid peroxidation by GPX4. Mechanistically, our data support a model in which myristoylation targets FSP1 to the plasma membrane where it mediates the NADH-dependent reduction of CoQ, which functions as a radical-trapping antioxidant that suppresses the propagation of lipid peroxides (Fig. 4h). Our data also reveal that a fundamental role of non-mitochondrial CoQ is to function as an antioxidant that prevents lipid damage, and consequently ferroptosis. Localization of FSP1 at lipid droplets is not required for protection from ferroptosis. One possibility is that the FSP1-mediated regulation of lipophilic radical-trapping antioxidants in lipid droplets is important for the maintenance of lipid quality during prolonged periods of lipid storage, similar to the function of CoQ and tocopherol in preventing the oxidation of circulating lipoprotein particles^{25,26}. Finally, our findings indicate that FSP1 expression is important for predicting the efficacy of ferroptosis-inducing drugs in cancers and highlight the potential for FSP1 inhibitors²³ as a strategy to overcome ferroptosis resistance in multiple types of cancer.

Online content

Any methods, additional references, Nature Research reporting summaries, source data, extended data, supplementary information, acknowledgements, peer review information; details of author contributions and competing interests; and statements of data and code availability are available at <https://doi.org/10.1038/s41586-019-1705-2>.

1. Dixon, S. J. et al. Ferroptosis: an iron-dependent form of nonapoptotic cell death. *Cell* **149**, 1060–1072 (2012).
2. Stockwell, B. R. et al. Ferroptosis: a regulated cell death nexus linking metabolism, redox biology, and disease. *Cell* **171**, 273–285 (2017).
3. Yang, W. S. et al. Regulation of ferroptotic cancer cell death by GPX4. *Cell* **156**, 317–331 (2014).
4. Ingold, I. et al. Selenium utilization by GPX4 is required to prevent hydroperoxide-induced ferroptosis. *Cell* **172**, 409–422.e21 (2018).
5. Dixon, S. J. & Stockwell, B. R. The hallmarks of ferroptosis. *Annu. Rev. Cancer Biol.* **3**, 35–54 (2019).
6. Zou, Y. et al. A GPX4-dependent cancer cell state underlies the clear-cell morphology and confers sensitivity to ferroptosis. *Nat. Commun.* **10**, 1617 (2019).
7. Wu, M., Xu, L.-G., Li, X., Zhai, Z. & Shu, H.-B. AMID, an apoptosis-inducing factor-homologous mitochondrion-associated protein, induces caspase-independent apoptosis. *J. Biol. Chem.* **277**, 25617–25623 (2002).
8. Ohiro, Y. et al. A novel p53-inducible apoptogenic gene, PRG3, encodes a homologue of the apoptosis-inducing factor (AIF). *FEBS Lett.* **524**, 163–171 (2002).
9. Dixon, S. J. et al. Pharmacological inhibition of cysteine–glutamate exchange induces endoplasmic reticulum stress and ferroptosis. *eLife* **3**, e02523 (2014).
10. Bersuker, K. et al. A Proximity labeling strategy provides insights into the composition and dynamics of lipid droplet proteomes. *Dev. Cell* **44**, 97–112.e7 (2018).
11. Magtanong, L. et al. Exogenous monounsaturated fatty acids promote a ferroptosis-resistant cell state. *Cell Chem. Biol.* **26**, 420–432.e9 (2019).
12. Yang, W. S. et al. Peroxidation of polyunsaturated fatty acids by lipoxygenases drives ferroptosis. *Proc. Natl. Acad. Sci. USA* **113**, E4966–E4975 (2016).
13. Marshall, K. R. et al. The human apoptosis-inducing protein AMID is an oxidoreductase with a modified flavin cofactor and DNA binding activity. *J. Biol. Chem.* **280**, 30735–30740 (2005).
14. Shimada, K. et al. Global survey of cell death mechanisms reveals metabolic regulation of ferroptosis. *Nat. Chem. Biol.* **12**, 497–503 (2016).
15. Arroyo, A., Navarro, F., Navas, P. & Villalba, J. M. Ubiquinol regeneration by plasma membrane ubiquinone reductase. *Protoplasma* **205**, 107–113 (1998).
16. Takahashi, T., Okamoto, T., Mori, K., Sayo, H. & Kishi, T. Distribution of ubiquinone and ubiquinol homologues in rat tissues and subcellular fractions. *Lipids* **28**, 803–809 (1993).
17. Sun, X. et al. Activation of the p62-Keap1-NRF2 pathway protects against ferroptosis in hepatocellular carcinoma cells. *Hepatology* **63**, 173–184 (2016).
18. Rees, M. G. et al. Correlating chemical sensitivity and basal gene expression reveals mechanism of action. *Nat. Chem. Biol.* **12**, 109–116 (2016).
19. Hanguer, M. J. et al. Drug-tolerant persister cancer cells are vulnerable to GPX4 inhibition. *Nature* **551**, 247–250 (2017).
20. Viswanathan, V. S. et al. Dependency of a therapy-resistant state of cancer cells on a lipid peroxidase pathway. *Nature* **547**, 453–457 (2017).
21. Zhang, Y. et al. Imidazole ketone erastin induces ferroptosis and slows tumor growth in a mouse lymphoma model. *Cell Chem. Biol.* **26**, 623–633.e9 (2019).
22. Hayano, M., Yang, W. S., Corn, C. K., Pagano, N. C. & Stockwell, B. R. Loss of cysteinyl-tRNA synthetase (CARS) induces the transsulfuration pathway and inhibits ferroptosis induced by cystine deprivation. *Cell Death Differ.* **23**, 270–278 (2016).
23. Doll, S. et al. FSP1 is a glutathione-independent ferroptosis suppressor. *Nature* <https://doi.org/10.1038/s41586-019-1707-0> (2019).
24. Nguyen, T. B. et al. DGAT1-dependent lipid droplet biogenesis protects mitochondrial function during starvation-induced autophagy. *Dev. Cell* **42**, 9–21.e5 (2017).
25. Tribble, D. L. et al. Oxidative susceptibility of low density lipoprotein subfractions is related to their ubiquinol-10 and α-tocopherol content. *Proc. Natl. Acad. Sci. USA* **91**, 1183–1187 (1994).
26. Stocker, R., Bowry, V. W. & Frei, B. Ubiquinol-10 protects human low density lipoprotein more efficiently against lipid peroxidation than does α-tocopherol. *Proc. Natl. Acad. Sci. USA* **88**, 1646–1650 (1991).

Publisher's note Springer Nature remains neutral with regard to jurisdictional claims in published maps and institutional affiliations.

© The Author(s), under exclusive licence to Springer Nature Limited 2019

Methods

No statistical methods were used to predetermine sample size. The experiments were not randomized and investigators were not blinded to allocation during experiments and outcome assessment.

Cell lines and culture conditions

U-2 OS T-Rex Flp-In cells, a gift from D. Durocher, and U-2 OS Tet-On cells (Clontech) were cultured in DMEM containing 4.5 g/l glucose and L-glutamine (Corning). NCI-H460, NCI-H2291, NCI-H1703 and NCI-H446 cells (ATCC) were cultured in RPMI1640 containing high glucose, L-glutamine and HEPES (ATCC). U-2 OS COQ2^{KO} cells were grown in DMEM supplemented with 200 µM uridine and FSP1^{KO} COQ2^{KO} cells were grown in DMEM supplemented with 200 µM uridine and 1 µg/ml Fer1. NCI-H460 GPX4^{KO} lines and FSP1^{KO} GPX4^{KO} lines were grown in RPMI1640 supplemented with 1 µg/ml Fer1. All media were supplemented with 10% fetal bovine serum (FBS, Thermo Fisher Scientific and Gemini Bio Products), and all cell lines were grown at 37 °C with 5% CO₂. All cell lines were tested for mycoplasma and were not authenticated.

Generation of doxycycline-inducible cell lines

U-2 OS expression lines were generated by transfection of U-2 OS T-Rex Flp-In cells with pOG44 Flp-Recombinase plasmid (Thermo Fisher Scientific) and pcDNA5/FRT/TO plasmid at a 9:1 ratio, followed by selection in 500 µg/ml hygromycin. NCI-H1703 and NCI-H446 expression lines were generated by infection with pLenti CMV TetR Blast virus (716-1) (Addgene plasmid no. 17492) in the presence of 8 µg/ml polybrene (Sigma-Aldrich), followed by selection in medium containing 2 µg/ml blasticidin for NCI-H1703 cells and 0.5 µg/ml blasticidin for NCI-H446 cells. TetR cells were subsequently infected with pLenti CMV/TO Hygro DEST virus (670-1) (Addgene plasmid no. 17293) containing the FSP1-GFP construct and were selected in medium containing 250 µg/ml hygromycin. FSP1-GFP-expressing cells were enriched by fluorescence-activated cell sorting of the GFP-positive populations.

Generation of CRISPR-Cas9 genome-edited cell lines

For the CRISPR-Cas9 synthetic lethal screen, U-2 OS Tet-On lines stably expressing Cas9 were generated by infection with lentiCas9-Blast, a gift from F. Zhang (Addgene plasmid no. 52962) and cells were selected in medium containing 1 µg/ml blasticidin. Active Cas9 expression was validated by flow cytometry analysis following infection with a self-cutting mCherry plasmid, which expresses mCherry and an sgRNA targeting the mCherry gene.

U-2 OS FSP1^{KO} lines were generated using CRISPR-Cas9 technology by transfection with pSpCas9(BB)-2A-Puro (PX459), a gift from F. Zhang (Addgene plasmid no. 48139), followed by selection in medium containing 1 µg/ml puromycin and isolation of individual clones using cloning rings. U-2 OS COQ2^{KO} and FSP1^{KO} COQ2^{KO}, FSP1^{KO} ACSL4^{KO} and FSP1^{KO} NQO1^{KO} lines were generated by cotransfected an FSP1^{KO} clonal line (FSP1 sgRNA guide 1, described in 'Plasmids') with PX459 plasmids encoding the appropriate guides, together with pcDNA3.1/Hygro(-) (Thermo Fisher Scientific) at a 20:1 w/w ratio, selection in medium containing 500 µg/ml hygromycin, and isolation of individual clones using cloning rings. U-2 OS FSP1-HaloTag knock-in lines were generated by cotransfection of U-2 OS T-Rex Flp-In cells with the donor plasmid pUC57 (described in 'Plasmids') and PX459 encoding FSP1 sgRNA guide 3 at a 2:1 w/w ratio in medium containing 1 µM SCR7 non-homologous end joining inhibitor (Xcess Biosciences) for 48 h, followed by selection in medium containing 1 µg/ml puromycin.

NCI-H460 FSP1^{KO} lines were generated by infection with lentiCRISPR v2-Blast (Addgene plasmid no. 83489) virus, selection in medium containing 2 µg/ml blasticidin and isolation of single clones using cloning rings. NCI-H460 GPX4^{KO} lines and FSP1^{KO} GPX4^{KO} lines were generated by infection with lentiCRISPR v2-Hygro (Addgene plasmid no. 98291)

virus, selection in medium containing 250 µg/ml hygromycin, and isolation of single clones using cloning rings.

Plasmids

Cloning of all expression plasmids and the HaloTag donor plasmid was performed using restriction enzyme-independent fragment insertion by polymerase incomplete primer extension. To generate the FSP1-HaloTag knock-in donor plasmid, 800-base-pair homology arms flanking the FSP1 stop codon were amplified from U-2 OS genomic DNA and inserted in frame 5' and 3' to the linker-TEV-HaloTag sequence in pUC57 (a gift from R. Tjian). The protospacer adjacent motif site that corresponds to FSP1 sgRNA guide 3 was subsequently mutated in the donor sequence using mutagenesis primers to prevent cutting of the integrated donor sequence by Cas9. FSP1(WT)-GFP was generated by insertion of FSP1-GFP in pDEST47¹⁰ into pcDNA5/FRT/TO, and FSP1(G2A)-GFP and FSP1(E156A)-GFP were subsequently generated using site-directed mutagenesis. TOM20(SS)-FSP1(G2A)-GFP and LYN11-FSP1(G2A)-GFP were generated by insertion of the signal sequence of TOM20 and the first 11 amino acids of LYN kinase, respectively, at the N terminus of FSP1(G2A)-GFP. FSP1(G2A)-GFP-PLIN2 and FSP1(G2A)-GFP-Cb5 were generated by insertion of the full-length sequence for PLIN2 and amino acids 100–134 of cytochrome b5, respectively, at the C terminus of FSP1(G2A)-GFP. LYN11-mCherry-FRB was generated by replacement of CFP in LYN11-CFP-FRB²⁷ with the sequence for mCherry. BFP-Sec61 was a kind gift from G. Voeltz. FSP1-GFP in pLenti CMV/TO Hygro DEST (Addgene no. 17291) was generated by insertion of FSP1-GFP into pENTR1A, followed by Gateway recombination cloning (Thermo Fisher Scientific). NQO1-GFP was generated by PCR amplification of NQO1 from U-2 OS cDNA and insertion into pcDNA5/FRT/TO encoding GFP. LYN11-NQO1-GFP was generated by insertion of amino acids 1–11 of LYN at the N terminus of NQO1-GFP. For protein expression, FSP1(WT) and FSP1(E156A) lacking the ATG start codon were inserted into the pET-His6-TEV vector (Addgene plasmid no. 29653), C-terminal to the His6-TEV tag. LentiCas9-Blast was developed by the Zhang laboratory.

Plasmid transfections were performed in U-2 OS cells with FuGene6 (Promega) transfection reagent. Virus was produced by cotransfection of HEK293T cells with GAG, POL and pLenti expression plasmids at a 1:1:1 w/w/w ratio, using the X-tremeGENE HP (Roche) transfection reagent. Medium containing secreted virus was collected after 48 h and sterile-filtered.

CRISPR guide RNA (sgRNA) sequences targeting FSP1, ACSL4, NQO1, GPX4 and COQ2 were designed using the CRISPR design tool developed by the Zhang laboratory, available online (<http://crispr.mit.edu/>). The oligonucleotide sequences preceding the protospacer motif were: FSP1 guide 1, 5' caccgGAATCGGGAGCTCTGCACG 3'; FSP1 guide 2, 5' caccgTC-CCGATTCCACCGAGACCT 3'; FSP1 guide 3, 5' caccgTGAGGCAGTCTCACCTTGA 3'; ACSL4 guide 1, 5' caccgTGCAATCATCCATTGGCCCC 3'; ACSL4 guide 2, 5' caccgTGGTAGTGGACTCACTGCAC 3'; NQO1 guide 1, 5' caccgTTTGCAGCACTCACCGACCA 3'; NQO1 guide 2, 5' caccgCAGAGGCACTGATCGTAC 3'; COQ2 guide, 5' caccgATGCTGGGCTCGC-GAGCCGC 3'; and GPX4 guide, 5' caccgAGCCCCGCCGATGAGCT 3'.

Nucleotides in lowercase show the overhangs introduced into oligonucleotides that are necessary for cloning into the BbsI restriction site of vector PX459 or BsmBI site of lentiCRISPR v2.

Chemicals and reagents

Reagents used in this study include: RSL3 (Cayman Chemical), Fer1 (Cayman Chemical), idebenone (Cayman Chemical), DFO (Cayman Chemical), doxycycline (Sigma), erastin2 (also known as compound 35MEW28) (synthesized by Acme), ML162 (Cayman Chemical), ZVAD(OMe)-FMK (Cayman Chemical), necrostatin-1 (Cayman Chemical), puromycin (Thermo Fisher Scientific), nutlin-3 (Cayman Chemical), CellEvent caspase-3/7 Green Detection Reagent (Thermo Fisher Scientific), etoposide (Sigma-Aldrich), rotenone (Sigma-Aldrich), blasticidin (Thermo

Article

Fisher Scientific), BODIPY 558/568 C12 (Thermo Fisher Scientific), BODIPY 493/503 (Thermo Fisher Scientific), BODIPY 581/591 C11 (Thermo Fisher Scientific), NMT inhibitor DDD85646 (Aobious), 4-CBA (Sigma-Aldrich), OptiPrep (Sigma-Aldrich), SYTOX Green Dead Cell Stain (Thermo Fisher Scientific), MitoTracker Green FM (Thermo Fisher Scientific), MitoTracker Orange CMTMRos (Thermo Fisher Scientific), CellMask Deep Red (Thermo Fisher Scientific), JF549 (kind gift from L. Lavis), oleate (Sigma-Aldrich), polybrene (Sigma-Aldrich), myristate (Sigma-Aldrich), YnMyr (Iris Biotech), AutoDOT (Abgent), DGAT1 inhibitor T863 (Sigma-Aldrich), DGAT2 inhibitor PF-06424439 (Sigma-Aldrich), SCR7 non-homologous end joining inhibitor (Xcess Biosciences), TAMRA-azide-PEG-biotin (BroadPharm), coenzyme Q₁ (Sigma-Aldrich), resazurin (Thermo Fisher Scientific) and NADH (Sigma-Aldrich). IKE was synthesized as previously described²¹.

Cell death analysis

Cells were plated in triplicate at a density of 2,000–3,000 cells per well in black 96-well plates (Corning) 48 h before start of imaging. To induce expression of FSP1, cells were treated with 10 ng/ml doxycycline at the time of plating. After 48 h, the medium was replaced with fresh medium containing 30 nM SYTOX Green Dead Cell Stain, doxycycline (if needed) and the indicated drugs. The plates were immediately transferred to an IncuCyte Zoom imaging system (Essen Bioscience) enclosed in an incubator set to 37 °C and 5% CO₂. Three images per well were captured in the green and phase channels every 1 or 2 h over a 48 h period, and the ratio of SYTOX Green-positive objects (dead cells) to phase objects (total cells) was quantified using Zoom image analysis software (Essen Bioscience). For each treatment condition, the SYTOX-to-phase-object ratio was plotted against the 48 h imaging interval, the AUC was calculated, and the average AUC was plotted as a function of drug concentration (for example, RSL3) using Prism (GraphPad). To calculate the half-maximal effective concentration (EC₅₀) values, the AUC curve was fit to a variable slope function comparing response to drug concentration. To quantify death in NQO1^{KO} cells, NQO1^{KO} FSP1^{KO} cells and lung cancer lines, SYTOX counts were used to calculate the AUC. To compare cell death between parental lung cell lines, the AUC values were normalized by the maximum value for each cell line.

For the 4-CBA treatment experiments, cells were treated with vehicle (1% v/v ethanol) or 3 mM 4-CBA 24 h after plating. Forty-eight hours after plating, the medium was replaced with fresh medium containing 4-CBA and the indicated drugs. For experiments comparing control to COQ2^{KO} cells, all cells were cultured in 200 μM uridine during imaging.

Western blotting

Cells were washed twice with PBS, lysed in 1% SDS, sonicated for 10 s and incubated for 5 min at 100 °C. Protein concentrations were determined using the bicinchoninic acid (BCA) protein assay (Thermo Fisher Scientific), and equal amounts of protein by weight were combined with 1× Laemmli buffer, separated on 4–20% polyacrylamide gradient gels (Bio-Rad Laboratories) and transferred onto nitrocellulose membranes (Bio-Rad Laboratories). Membranes were washed in PBS with 0.1% Tween-20 (PBST) and blocked in PBST containing 5% (w/v) dried milk for 30 min. Membranes were incubated for 24 h in PBST containing 5% bovine serum albumin (BSA) (Sigma Aldrich) and primary antibodies. After washing with PBST, membranes were incubated at room temperature for 30 min in 5% BSA and PBST containing fluorescent secondary antibodies. Immunoblots were imaged on a LI-COR imager (LI-COR Biosciences).

The following blotting reagents and antibodies were used: anti-PLIN2 (Abgent), anti-AIFM2 (Proteintech Group and Santa Cruz Biotechnology), anti-α-tubulin (Cell Signaling Technology and Santa Cruz Biotechnology), anti-GPX4 (Abcam), anti-ACSL4 (Sigma-Aldrich), anti-GFP (Proteintech Group), anti-NQO1 (Proteintech Group), anti-GAPDH (EMD Millipore), anti-RAS (Cell Biolabs), anti-MDR1 (Cell Signaling Technology), anti-p21 (Cell Signaling Technology), anti-rabbit IRDye800

conjugated secondary (LI-COR Biosciences) and anti-mouse Alexa Fluor 680 conjugated secondary (Invitrogen).

Fluorescence microscopy

For fluorescence microscopy of PLIN2 and FSP1-GFP in fixed cells, cells grown on coverslips were treated with 200 μM oleate-BSA complex for 24 h, washed 3× with PBS, fixed for 15 min in PBS containing 4% (w/v) paraformaldehyde and washed 3× again with PBS. Cells were permeabilized for 15 min with blocking solution (1% BSA and PBS) containing 0.01% digitonin, washed 3× and incubated in blocking solution for an additional 15 min. Cells were incubated with anti-PLIN2 antibody in blocking solution (1:500 dilution) for 2 h at room temperature, washed 3× and incubated for 1 h in blocking solution containing anti-rabbit secondary antibody conjugated to Alexa Fluor 594 (1:500 dilution) (Thermo Fisher Scientific). After additional 3× washes, coverslips were mounted on glass slides using Fluoromount G (Southern Biotech). For fluorescence microscopy of FSP1-GFP and LYN-mCherry-FRB, cells were fixed in PBS containing 4% (w/v) paraformaldehyde and washed 3× with PBS before mounting.

For live-cell microscopy, cells were grown in 4-well or 8-well Laboratory-Tek II Chambered Coverglass (Thermo Fisher Scientific) imaging chambers. To image lipid droplets, cells were incubated for 24 h with 1 μM BODIPY 558/568 C12 (Thermo Fisher Scientific) or treated with 100 μM AutoDOT before imaging. To image the cell membrane, cells were incubated with 5 μg/ml CellMask Deep Red for 30 min, and the medium was replaced before imaging. To image mitochondria, cells were incubated with 100 nM MitoTracker Orange CMTMRos or MitoTracker Green FM for 15 min. For imaging that required prior transfection, cells were transiently transfected with the indicated plasmids in 6-well plates using Fugene6, incubated for 48 h and seeded in Laboratory-Tek II chambers before imaging. To image FSP1-HaloTag, cells were incubated with 100 nM JF549 dye for 30 min, washed 3× with PBS and imaged in fresh medium.

Cells were imaged using a Deltavision Elite widefield epifluorescence deconvolution microscope (GE Healthcare) equipped with a 60× oil immersion objective (Olympus), using DAPI, FITC, Tx-Red and Cy5 filters. For live-cell microscopy, cells were imaged in an enclosure heated to 37 °C and exposed to a continuous perfusion of a gas mixture containing 5% CO₂, 21% O₂ and 74% N₂ (BioBlend, Praxair). Z-stacks of 0.2-μm slices totalling 4–6 μm in thickness were acquired for deconvolution using SoftWoRx software (GE Life Sciences). Single deconvolved slices for each channel were analysed and merged using ImageJ (<http://imagej.nih.gov/ij/>).

Lipid droplet fractionation

Ten 15-cm plates of U-2 OS cells expressing inducible FSP1-GFP were induced with 10 ng/ml doxycycline for 48 h. Cells were collected by scraping into PBS and centrifuged for 10 min at 500g. Cell pellets were resuspended in cold hypotonic lysis medium (HLM, 20 mM Tris-HCl pH 7.4 and 1 mM EDTA) supplemented with 1× cComplete, Mini, EDTA-free Protease Inhibitor Cocktail (Sigma-Aldrich), incubated on ice for 10 min, dounced using 80× strokes and centrifuged at 1,000g for 10 min. The supernatant was subsequently transferred to Ultra-Clear ultracentrifuge tubes (Beckman-Coulter), diluted with 60% sucrose and HLM to a final concentration of 20% sucrose and HLM, and overlaid by 4 ml of 5% sucrose and HLM followed by 4 ml of HLM. Overlaid samples were centrifuged for 30 min at 15,000g in an ultracentrifuge using a SW41 swinging bucket rotor (Beckman-Coulter). Buoyant fractions were collected using a tube slicer (Beckman-Coulter), additional fractions were pipetted from the top of the sucrose gradient in 1-ml increments, and pellets were resuspended in 1 ml HLM. One hundred microlitres of 10% SDS was added to each fraction, yielding a final concentration of 1% SDS. Samples were then sonicated for 15 s and incubated for 10 min at 65 °C. Buoyant fractions were incubated at 37 °C for 1 h and sonicated every 20 min, followed by a final incubation at 65 °C for 10 min.

Plasma-membrane fractionation

Plasma-membrane subdomains were separated using a continuous OptiPrep gradient as previously described²⁸. Six 15-cm plates of cells expressing inducible FSP1–GFP were incubated with 10 ng/ml doxycycline for 48 h and collected by scraping into PBS, centrifuged for 10 min at 500g and resuspended in 1 ml of base buffer (20 mM Tris-HCl pH 7.8 and 250 mM sucrose) supplemented with 1 mM MgCl₂, 1 mM CaCl₂, and 1× cComplete, Mini, EDTA-free Protease Inhibitor Cocktail. Cells were passed 40× through a 1.5" 22-gauge needle and centrifuged at 1,000g for 10 min. The supernatant was retained, and the pellet was resuspended in an additional 1 ml base buffer containing 1 mM MgCl₂ and 1 mM CaCl₂. The resuspended pellet was passed 40× through a 22-gauge needle, centrifuged at 1,000g for 10 min and the supernatant was combined with 1 ml of supernatant from the previous step to make 2 ml in total. OptiPrep mixing solution was prepared by combining 60% OptiPrep stock solution with buffer containing 120 mM Tris-HCl pH 7.8 and 250 mM sucrose in a 5:1 v/v ratio. Two millilitres OptiPrep mixing solution was combined with 2 ml of sample supernatant from the previous centrifugation steps to yield 4 ml of a sample containing 25% OptiPrep. This OptiPrep-mixed sample was gently pipetted under 8 ml of a continuous 5–20% OptiPrep gradient prepared in base buffer in an UltraClear tube. The loaded sample was subsequently centrifuged for 90 min at 52,000g at 4 °C using a SW41 swinging bucket rotor. After centrifugation, individual 0.67-ml fractions were collected by pipetting from the top of the gradient and analysed by western blot. The plasma-membrane-localized proteins RAS and MDR1 were used as markers of plasma-membrane fractions.

CRISPR–Cas9 synthetic lethal screen

The CRISPR–Cas9 screen was performed as previously described²⁹. The ‘Apoptosis and Cancer’ sublibrary of sgRNAs²⁹ comprising 31,324 elements—including 29,824 sgRNAs targeting 3,015 genes (about 10 sgRNAs per gene) and 1,500 negative-control sgRNAs—was used. To generate lentiviral particles, the sublibrary was co-transfected with third-generation lentiviral packaging plasmids (pVSVC, pRSV and pMDL) into HEK293T cells. Medium containing lentivirus was collected 48 and 72 h after transfection, combined, filtered and then used to infect about 2.1×10^7 U-2 OS Tet-On cells stably expressing Cas9. After 72 h of growth, infected cells were selected in medium containing 1 µg/ml puromycin until over 90% cells were mCherry-positive. Cells were then re-seeded in 500-cm² plates (about 8×10^6 cells per plate) and recovered in medium lacking puromycin for 24 h. For the screen, a total of about 3.2×10^7 cells (that is, about 1,000-fold library coverage) were treated with either DMSO or 0.5 µM RSL3 for 5 days. Cells were then trypsinized, collected by centrifugation at 1,000g, washed twice with PBS and pellets were frozen at -80 °C. Genomic DNA was extracted using the QIAamp DNA Blood Maxi Kit (QIAGEN) according to the manufacturer’s instructions. sgRNA sequence libraries were prepared from genomic DNA by two rounds of PCR using the Herculase II Fusion DNA Polymerase (Agilent). sgRNA sequences were amplified by the primers oMCB1562 and oMCB1563 and then indexed using the Illumina TruSeq LT adaptor sequences AD006 (GCCAAT; DMSO) or AD012 (CTTGTA; RSL-3) for downstream deep sequencing analysis. PCR products were separated on a 2% tris-borate-EDTA (TBE)-agarose gel, purified using the QIAquick Gel Extraction Kit (Qiagen) and assessed for quality using a Fragment Analyzer (Agilent). PCR amplicons from each sample were pooled in a 1:1 ratio based on their concentrations as determined by Qubit Fluorometric Quantification. sgRNA sequences were analysed by deep sequencing using the primer oMCB1672 on an Illumina MiSeq instrument at the Oklahoma Medical Research Foundation. Sequence reads were aligned to the sgRNA reference library using Bowtie software. For each gene, a gene effect and score (likely maximum effect size and score), and P value

were calculated using the casTLE statistical framework as previously described²⁹.

Click chemistry and in-gel fluorescence

To analyse myristoylated proteins in buoyant fractions enriched in lipid droplets, 2015-cm plates of U-2 OS cells were incubated with 100 µM myristic acid or 100 µM YnMyr for 48 h. Buoyant fractions were isolated by sucrose gradient fractionation as described in ‘Lipid droplet fractionation’, combined with SDS (1% final concentration) and dialysed into a 0.1% SDS and PBS solution. A click mixture was prepared by adding reagents in the following order, and by vortexing after the addition of each reagent: 10 µl of 10 mM TAMRA-azide-PEG-biotin (BroadPharm), 20 µl of 50 mM copper (II) sulfate, 20 µl of 50 mM tris(2-carboxyethyl)phosphine, 10 µl of 10 mM tris(benzyltriazolylmethyl) amine. Sixty microlitres of click mixture was then added to 1 ml of the dialysed samples. The samples were then vortexed and incubated for 1 h at room temperature. One millilitre of cold methanol containing 10 mM EDTA was added to each sample, and the samples were briefly vortexed and stored at -80 °C overnight. The following day, the samples were centrifuged at 17,000g at 4 °C for 30 min to pellet precipitated proteins. Pellets were washed twice with 1 ml cold methanol, dried in a speed-vacuum centrifuge under medium heat, and resuspended in 80 µl PBS containing 1% SDS. Once dissolved, proteins were resuspended in 1× Laemmli loading buffer and analysed by SDS-PAGE. To visualize proteins using fluorescence, the gel was washed 3× with milliQ water and imaged using a ChemiDoc XRS+ Imaging System (Bio-Rad Laboratories).

To analyse myristoylated proteins in whole-cell lysates, U-2 OS cells were incubated with 100 µM myristic acid or 100 µM YnMyr for 48 h. Cells were washed twice with PBS and lysed in buffer containing 1% SDS and PBS and 1× EDTA-free complete protease inhibitor. Equal amounts of protein by weight were diluted to 0.1% SDS and PBS and subjected to click chemistry with TAMRA-azide-PEG-biotin.

Enrichment of N-myristoylated proteins

YnMr-labelled proteins in cell lysates were conjugated to TAMRA-azide-PEG-biotin using click chemistry as described in ‘Click chemistry and in-gel fluorescence’. After protein precipitation in cold methanol, the pellet was resuspended in 80 µl of 1% SDS and PBS. Once the pellet was completely dissolved, 65 µl was diluted 10-fold with PBST. Fifteen microlitres of Streptavidin Agarose Resin (Thermo Fisher Scientific) was washed 3× with PBST. The diluted sample was added to the bead resin and rotated for 3 h at room temperature. Beads were washed 5× with PBST and bound proteins were eluted by boiling the beads for 5 min in 2× Laemmli buffer containing 2 mM biotin.

Lipidomic profiling using liquid chromatography–tandem mass spectrometry

Cas9^{ctd} and FSP1^{KO} U-2 OS cells grown in 10-cm plates were scraped into PBS, centrifuged at 500g for 5 min, and processed as previously described²⁴. After addition of internal standards (10 nmol of dodecylglycerol and 10 nmol of pentadecanoic acid), lipids were extracted in a 4 ml solution of 2:1:1 choloroform:methanol:PBS. The organic and aqueous layers were separated by centrifugation at 1,000g for 5 min. Following the collection of the organic layer, the remaining organic material in the aqueous layer was acidified by addition of 0.1% formic acid and re-extracted with 2 ml of chloroform. Extracts were combined, dried down under a stream of nitrogen and then resolubilized in 120 µl of chloroform. Ten microlitres of sample was analysed by single reaction monitoring-based liquid chromatography–mass spectrometry. Liquid chromatography separation was performed using a Luna reverse-phase C5 column, and mass spectrometry analysis was preformed using an Agilent 6400 triple quadrupole (QQQ)–liquid chromatography–mass spectrometry instrument. Metabolites were quantified by integrating the AUC, and the values were normalized to the internal standards.

Glutathione measurements

The day before the experiment, 2×10^5 Cas9^{ctl} and FSP1^{KO} U-2 OS cells per well were seeded into 6-well dishes. Cells were treated with DMSO (vehicle), erastin2 (1 μ M) for 6 h or RSL3 (250 nM) for 1 h. Cells were collected by scraping and prepared for measurement of glutathione (GSH + GSSG) using the Cayman Chemical Glutathione Assay Kit (Cayman Chemical) according to the manufacturer's protocol. The GSH and GSSG concentrations were calculated using a standard curve and normalized to the total protein level in each sample. Three independent biological replicates were performed for each condition.

BODIPY 581/591 C11 analysis

The day before the experiment, 2×10^5 U-2 OS cells per well were seeded into 6-well dishes containing a 22-mm² glass coverslip in each well. Cells were treated with DMSO (vehicle) or RSL3 (250 nM) for 75 min. At the end of the treatment, the treatment medium was removed and cells were washed once with HBSS. Cells were then labelled in 1 ml HBSS containing 5 μ M BODIPY 581/591 C11 and incubated at 37 °C for 10 min. The label mixture was removed and 1 ml of fresh HBSS was added to the cells. The cover slip was transferred to a glass microscope slide onto which 25 μ l of fresh HBSS had been applied. Confocal imaging and quantification of BODIPY 581/591 C11 were performed as previously described¹¹ on two independent biological replicates per treatment. Using ImageJ, each nucleus was attributed two regions of interest (ROI), one perinuclear and one plasma membrane-localized. Red and green fluorescence values were quantified for each ROI and corrected for background by subtracting the red or green fluorescence in cell-free areas. The BODIPY 581/591 C11 value was calculated as the ratio of the green fluorescence (which indicates oxidized probe) to total (green + red, which indicates total reduced plus oxidized probe) fluorescence.

Tumour xenograft growth studies

For Fer1 withdrawal experiments, tumour xenografts were established by injection of GPX4^{KO} and GPX4^{KO} FSP1^{KO} H460 cells into the flank of male C.B17 SCID mice, 6 weeks of age (Taconic Farms) ($n = 8$). In brief, cells were washed with PBS, trypsinized and collected in serum-containing medium. Collected cells were then washed with serum-free medium once and resuspended in serum-free medium at a concentration of 2×10^4 cells/ μ l. One hundred microlitres of cells (2×10^6 cells) were injected per mouse. Fer1 was prepared at a concentration of 0.2 mg/ml in 18:1 v/v PBS:ethanol:PEG40. Mice were injected intraperitoneally with Fer1 daily (2 mg kg⁻¹ body weight), and tumour size was measured using callipers. Fer1 injections were discontinued in 1 set of mice 5 days after cell injection, and tumour size was measured once every 2 days in each mouse for an additional 17 days. Mice not included in the analysis included mice that were killed early owing to sickness ($n = 1$ of GPX4^{KO} (+) Fer1) and mice with tumours that were determined to be outliers according to the statistical test described in 'Statistical analysis and reproducibility' ($n = 1$ of GPX4^{KO} (-) Fer1 and $n = 1$ of GPX4^{KO} FSP1^{KO} (-) Fer1). The number of mice represented in the final analysis was GPX4^{KO} (-) Fer1 ($n = 7$), GPX4^{KO} (+) Fer1 ($n = 7$), GPX4^{KO} FSP1^{KO} (-) Fer1 ($n = 7$), and GPX4^{KO} FSP1^{KO} (+) Fer1 ($n = 8$).

For IKE injection experiments, IKE was resuspended at 4 mg/ml in an HBSS pH 4 solution containing 4% DMSO, 2% ethanol and 4% PEG40. To prepare this solution, 24 mg of IKE was dissolved in 200 μ l DMSO, and 100 μ l ethanol and 250 μ l PEG40 were sequentially added. This mixture was added to 5.4 ml of HBSS pH 4 (Gibco) and sterile-filtered. Tumour xenografts were established by injection of Cas9^{ctl} ($n = 8$) or FSP1^{KO} H460 ($n = 8$) cells. After 10 days, each group of mice ($n = 8$) was injected daily with vehicle or 40 mg kg⁻¹ IKE (250 μ l total volume), and the fold change in tumour size was measured over a 24-day period. Mice not included in the analysis included mice that were killed early owing to the development of exceedingly large tumours ($n = 1$ of Cas9^{ctl} (+) IKE,

$n = 3$ of Cas9^{ctl} (-) IKE, $n = 3$ of FSP1^{KO} (+) IKE and $n = 1$ of FSP1^{KO} (-) IKE), mice in which tumours did not initiate ($n = 2$ of Cas9^{KO} (+) IKE), and mice with tumours that were determined to be statistical outliers according to the test described in 'Statistical analysis and reproducibility' ($n = 1$ of Cas9^{ctl} (+) IKE, $n = 1$ of Cas9^{ctl} (-) IKE, $n = 1$ of FSP1^{KO} (+) IKE). The number of mice represented in the final analysis was Cas9^{ctl} (-) IKE ($n = 4$), Cas9^{ctl} (+) IKE ($n = 4$), FSP1^{KO} (-) IKE ($n = 7$) and FSP1^{KO} (+) IKE ($n = 4$).

No statistical tests were used to calculate sample size. Sample size was $n = 8$ for each treatment group to account for differences in tumour formation and growth, and to ensure recovery of a sufficient quantity of mice with tumours of approved size at each time point of the study. Following injection of H460 cells, the mice were randomly assigned into two treatment groups for the Fer1 withdrawal experiments and into two treatment groups for the IKE injection experiments. Fold change in tumour volume was statistically analysed using the unpaired, two-way t-test. Blinding was not possible because the experiments were performed by a single researcher. All mouse experiments were conducted in accordance with the guidelines of the Institutional Animal Care and Use Committees (IACUC) of the University of California, Berkeley. Animals were euthanized when the xenograft tumour size reached two centimetres in any two dimensions. No mouse exhibited severe loss of body weight (>15%) or evidence of infections or wounds.

TIRF microscopy

Cells were imaged at room temperature using a Nikon Ti-E inverted microscope (Nikon Instruments) outfitted with a TIRF 60 \times /1.49 NA oil objective, an Andor Laser Combiner and an electron-multiplying charge-coupled device camera (iXon ULTRA 897BV; Andor Technology). Samples were excited with a 488-nm laser line, and emission was collected through a single band-pass filter centred on 510 nm. All images were acquired using iQ3 acquisition software (Andor Technology). The depth of the evanescent field was approximately 150 nm.

CoQ measurements

CoQ measurements were performed as previously described³⁰. To simultaneously measure the reduced and oxidized form of CoQ, a cold butyl-hydroxytoluene (BHT) solution was added to prevent auto-oxidation at the beginning of sample extraction. One hundred microlitres of a cold BHT-in-propanol solution (5 mg/ml) and 600 μ l of cold 1-propanol were added to each tube containing cells in the frozen state. Immediately after this, the mixture was subjected to sonication for 2 min. Subsequently, 100 μ l of cold coenzyme Q₉ solution (2 μ g/ml), which was used as internal standard, was added, and the mixture was vortex-mixed for 1 min. It was then centrifuged for 10 min at 3,500 rpm and 1 °C, and the propanol organic supernatant layer was transferred to an autosampler vial. One-hundred-microlitre aliquots of the 1-propanol extract were immediately analysed, and the reduced and oxidized CoQ levels were determined using high-performance liquid chromatography (HPLC). HPLC analysis was performed using an automated Hitachi Chromaster system equipped with a Model 5110 quaternary pump, Model 5210 autosampler, Model 5310 column oven and ESA CouloChem III detector. The EZChrom Elite software (Agilent) was used for monitoring output signal and processing the results. The analytical column was a 150-mm \times 4.6-mm C18 column with 5- μ m spherical particles connected to a Security Guard equipped with a C18 cartridge (4-mm \times 3-mm).

Apoptosis activation assay

Cells grown in 6-cm plates were washed with PBS, trypsinized and centrifuged for 5 min at 500g. Cell pellets were resuspended in PBS containing 5% FBS and 5 μ M CellEvent caspase-3/7 Green Detection Reagent and were incubated for 30 min at 37 °C. Cells were analysed on a LSRFortessa (Becton Dickinson) flow cytometer, and the raw data were processed using the FlowJo software package (TreeStar). Apoptotic cells were gated using the same forward scatter threshold across all samples, and FITC fluorescence of the gated populations was determined.

Protein purification and activity assays

Expression vectors were transformed into Rosetta DE3 competent cells (EMD Millipore) and LB cultures were inoculated for overnight growth at 37 °C while shaking. The following day, the cultures were diluted 1:100 into 500 ml of LB and allowed to grow to an optical density at 600 nm (OD_{600}) of 0.5, at which point the incubator was set to start cooling to 20 °C. The cultures were grown further to an OD_{600} of 0.7 and induced with 1 mM Isopropyl β-D-1-thiogalactopyranoside (IPTG) overnight. Bacterial pellets were resuspended in 2 ml of cold lysis buffer containing 50 mM potassium phosphate pH 8.0, 300 mM potassium chloride, and 30 mM imidazole, supplemented with 1× cComplete, Mini, EDTA-free Protease Inhibitor Cocktail. The resuspended cells were sonicated 5× on ice at 50% power for 10 s, with 2-min incubations on ice in between sonifications, and were centrifuged at 20,000g for 15 min at 4 °C. The supernatant was combined with 200 μl of Ni-NTA agarose beads (Thermo Fisher Scientific) washed 3× with lysis buffer, and the supernatant–bead mixture was rotated for 1 h at 4 °C. The beads were subsequently washed 5× with cold lysis buffer, and bound proteins were eluted by incubating beads for 15 min in 500 μl of cold lysis buffer containing 250 mM imidazole while rotating. The eluted proteins were dialysed into PBS containing 10% glycerol and snap-frozen in liquid N₂. Protein concentration was determined by measuring the absorbance at 280 nm.

To measure NADH oxidation kinetics, recombinant FSP1 was combined with 500 μM NADH and 200 μM coenzyme Q₁₀ in a total volume of 100 μl PBS. A reduction in absorbance at 340 nm, corresponding to NADH oxidation, was determined over the course of 1 h. To measure resazurin reduction kinetics, recombinant FSP1 was combined with 500 μM NADH and 500 μM resazurin in a total volume of 100 μl PBS. Fluorescence (emission at 590 nm) corresponding to reduced resazurin was determined over the course of 1 h. All measurements were taken using a SpectraMax i3 Multi-Mode Platform plate reader (Molecular Devices).

Analysis of the CTRP dataset

Data for significant correlations between *FSP1* gene expression and resistance to RSL3, ML162 and ML210 were downloaded from the CTRP v2 website¹⁸. Data for non-haematopoietic cancer cells was extracted from the v21.data.gex_global_analysis.txt table and plotted using Prism.

Statistical analysis and reproducibility

All figures, including western blots, dose–response curves and enzymatic activity assay panels are representative of two biological replicates unless stated otherwise. Images are representative of at least $n=10$ imaged cells. *P*values for pairwise comparisons were calculated using the two tailed *t*-test. For comparison across multiple experimental groups, *P*values were calculated using one-way ANOVA, and adjusted using Bonferroni correction for multiple comparisons. For Fig. 4a, b and Extended Data Fig. 10a, b, the normalized z-scored Pearson correlation coefficients were obtained from CTRP v2 (<https://portals.broadinstitute.org/ctrp/>). For xenograft experiments, all mice were randomized following tumour-cell injection into treatment groups. Outliers were identified using the Grubbs method, and were removed from analyses. To compare between groups of mice in each time point, *P* values were calculated using the unpaired, two way *t*-test.

Reporting summary

Further information on research design is available in the Nature Research Reporting Summary linked to this paper.

Data availability

All data that support the conclusions in this manuscript are available from the corresponding author upon reasonable request. Raw data for Fig. 1 are provided in Supplementary Table 1. Raw data for Fig. 3 are provided in Supplementary Table 3. Raw data for Fig. 4 are provided in Supplementary Table 4, and are publicly available from the Cancer Cell Line Encyclopedia (<https://portals.broadinstitute.org/ccle>) and CTRP databases.

Code availability

The castTLE statistical framework software for analysis of data from the CRISPR screen can be accessed at www.bitbucket.org/dmorgens/castle/. Bowtie software can be accessed at www.bowtie-bio.sourceforge.net/bowtie2/index.shtml. MATLAB image analysis software to analyse lipid droplet distributions can be obtained at www.droplet-proteome.org.

27. Inoue, T., Heo, W. D., Grimley, J. S., Wandless, T. J. & Meyer, T. An inducible translocation strategy to rapidly activate and inhibit small GTPase signaling pathways. *Nat. Methods* **2**, 415–418 (2005).
28. Macdonald, J. L. & Pike, L. J. A simplified method for the preparation of detergent-free lipid rafts. *J. Lipid Res.* **46**, 1061–1067 (2005).
29. Morgens, D. W. et al. Genome-scale measurement of off-target activity using Cas9 toxicity in high-throughput screens. *Nat. Commun.* **8**, 15178 (2017).
30. Tang, P. H., Miles, M. V., DeGrauw, A., Hershey, A. & Pesce, A. HPLC analysis of reduced and oxidized coenzyme Q₁₀ in human plasma. *Clin. Chem.* **47**, 256–265 (2001).

Acknowledgements This research was supported by grants from the National Institutes of Health (R01GM12948 to J.A.O., R01GM122923 to S.J.D., P42 ES004705 to D.K.N. and 1DP2CA195761-01 to R.Z.). J.A.O. is a Chan Zuckerberg Biohub investigator. D.K.N. was supported by a Cancer Research ASPIRE award from the Mark Foundation. P.H.T. was supported by the Internal Research Fund of the Division of Pathology and Laboratory Medicine, Cincinnati Children's Hospital Medical Center. We thank P.-J. Ko (Stanford) for assistance with confocal imaging, and D. Leto (Stanford) and R. Kopito (Stanford) for helpful discussions.

Author contributions K.B. and J.A.O. conceived the project and designed the experiments. J.A.O. and K.B. wrote the manuscript. All authors read and edited the manuscript. K.B. performed the majority of the experiments. Z.L. and M.A.R. performed and analysed the CRISPR screen with guidance from M.C.B. K.B. prepared samples and R.Z. performed the TIRF microscopy. B.F. performed the lipidomics, and P.H.T. measured CoQ levels and redox state. J.H. performed the click chemistry myristylation experiments. S.J.D. and L.M. performed the glutathione measurements and C11 experiments. J.M.H. generated the overexpression and knockout lung cancer lines and analysed ferroptosis in these lines. D.K.N., J.M.H., B.F., and M.A.R. performed the xenograft experiments. T.J.M. and B.T. synthesized IKE.

Competing interests S.J.D. is a member of the scientific advisory board for Ferro Therapeutics.

Additional information

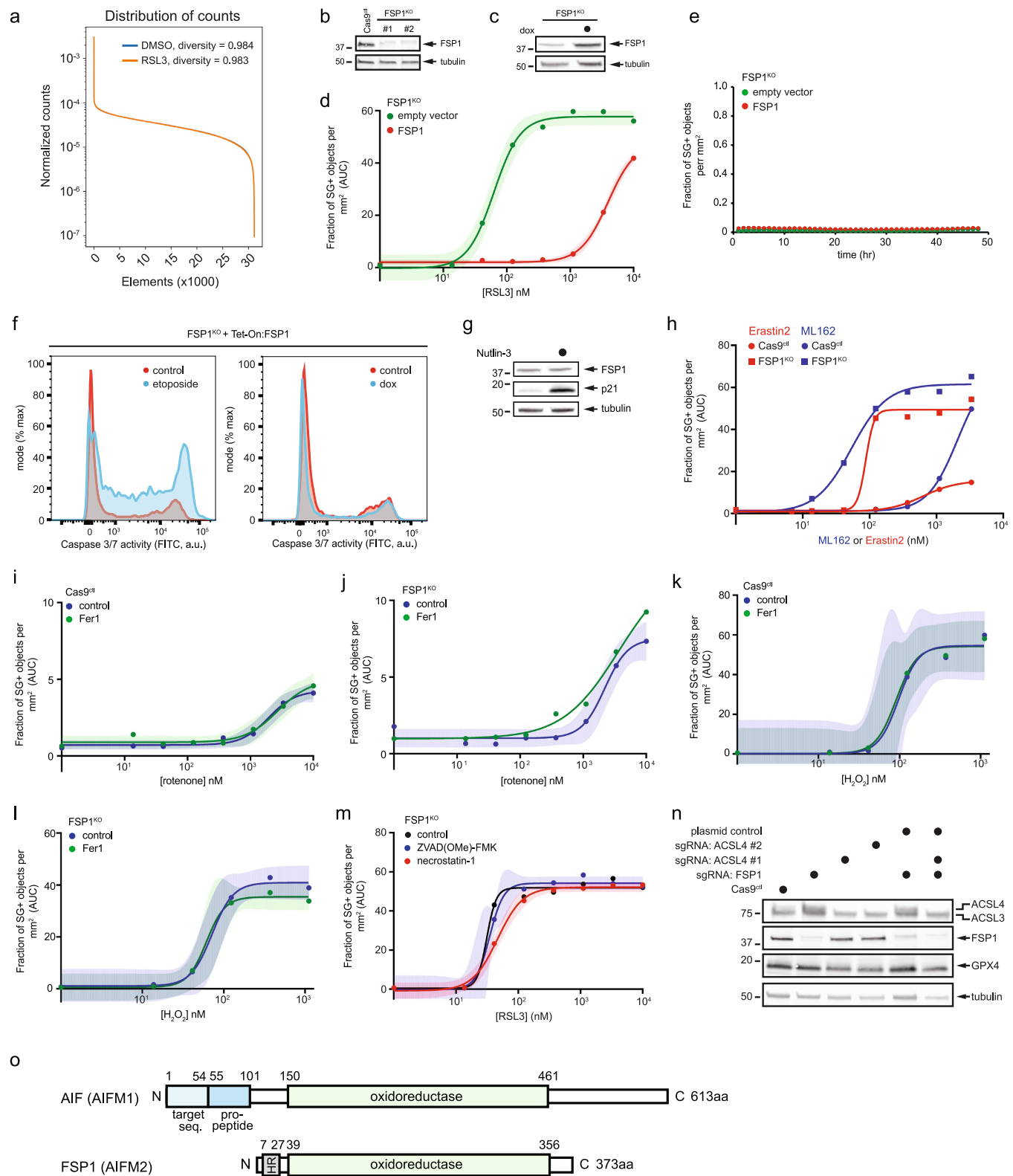
Supplementary information is available for this paper at <https://doi.org/10.1038/s41586-019-1705-2>.

Correspondence and requests for materials should be addressed to J.A.O.

Peer review information *Nature* thanks Kivanc Birsoy, Navdeep S. Chandel and the other, anonymous, reviewer(s) for their contribution to the peer review of this work.

Reprints and permissions information is available at <http://www.nature.com/reprints>.

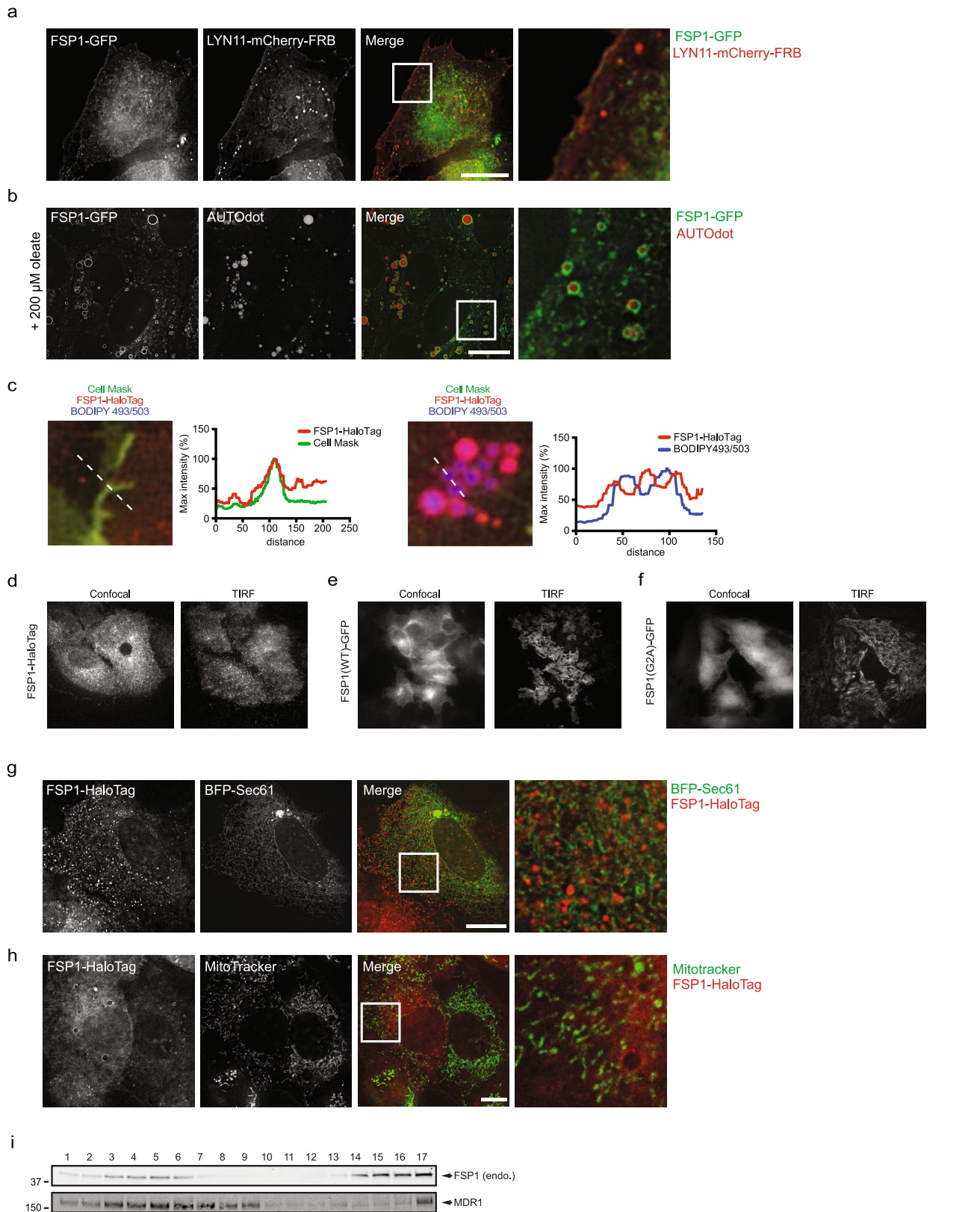
Article



Extended Data Fig. 1 | Synthetic lethal screen coverage and validation.

a, Distribution of counts across all sgRNA elements from the CRISPR–Cas9 screen. **b**, Western blot of control and FSP1^{KO} cells. **c**, **d**, Western blot analysis (**c**) and dose response of RSL3-induced death (**d**) of FSP1^{KO} cells that express doxycycline-inducible, untagged FSP1. **e**, Time-lapse analysis of cell death of FSP1^{KO} cells that express inducible, untagged FSP1. **f**, Flow cytometric analysis of caspase 3/7 activity in FSP1^{KO} cells that express inducible, untagged FSP1, treated with doxycycline for 48 h. As a positive control, non-induced cells were treated with 50 µM etoposide for 24 h before analysis. **g**, Western blot analysis of lysates from control cells treated with 10 µM nutlin-3 for 48 h. **h**, Dose

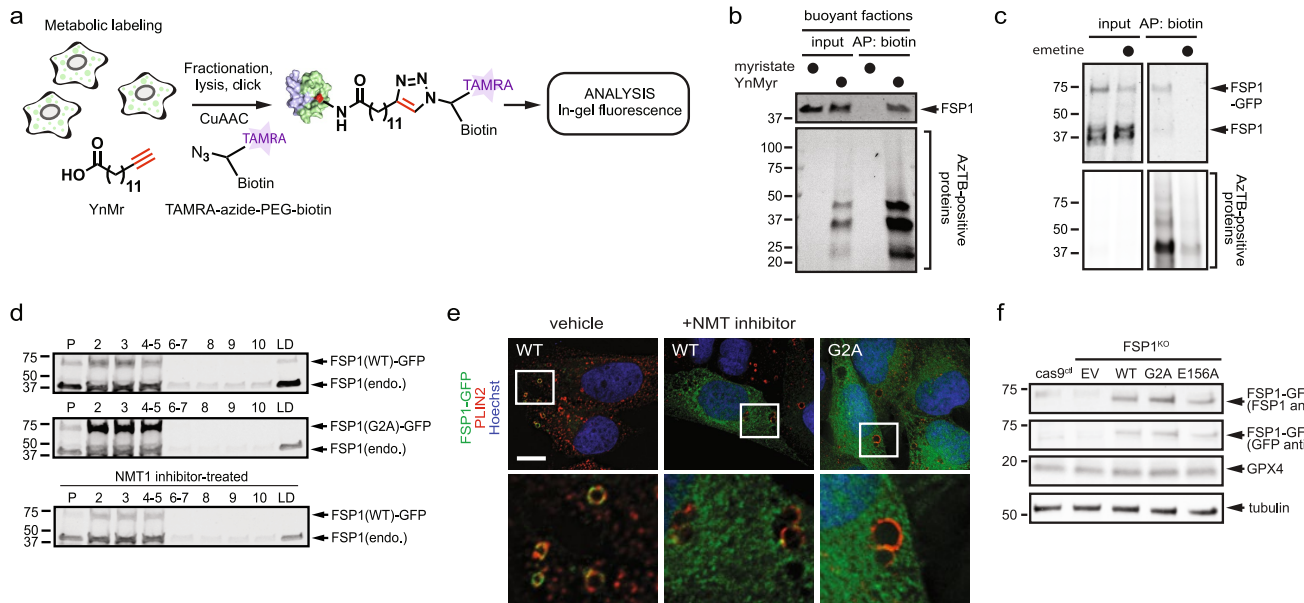
response of ML162 and erastin2-induced cell death. **i**, **j**, Dose response of rotenone-induced death of control (**i**) and FSP1^{KO} (**j**) cells. **k**, **l**, Dose response of hydrogen-peroxide-induced death of control (**k**) and FSP1^{KO} (**l**) cells. **m**, Dose response of RSL3-induced cell death in the presence of inhibitors of apoptosis (ZVAD(OMe)-FMK, 10 µM) and necroptosis (necrostatin-1, 1 µM). **n**, Western blot analysis of lysates from ACSL4^{KO} and FSP1^{KO} ACSL4^{KO} cells. **o**, Schematic of domains present in AIF and FSP1. In **d**–**m**, shading indicates 95% confidence intervals for the fitted curves and each data point is the average of three technical replicates. Panels are representative of two biological replicates, except panels **c**–**e** and **k**, **l**, which show single experiments.



Extended Data Fig. 2 | Subcellular distribution of FSP1. **a**, Inducible FSP1-GFP cells were transiently transfected with LYN11-mCherry-FRB for 24 h, induced with doxycycline for 48 h and fixed before imaging. **b**, FSP1-GFP cells were treated with 200 μM oleate for 24 h to induce lipid droplets and treated with 100 μM AutoDOT to label lipid droplets before imaging. **c**, Line intensity plots showing colocalization between FSP1-HaloTag and organelle markers. **d-f**, Confocal and TIRF microscopy of FSP1-HaloTag (**d**), and inducible

FSP1(WT)-GFP (**e**) and FSP1(G2A)-GFP (**f**) cells. **g**, FSP1-HaloTag cells were transiently transfected with BFP-Sec61 for 48 h before imaging to label the endoplasmic reticulum. **h**, FSP1-HaloTag cells were incubated with 100 nM MitoTracker Green FM to label mitochondria. **i**, Plasma-membrane subdomains from control cells were enriched by OptiPrep gradient centrifugation. Endo., endogenous FSP1. Western blot is representative of two biological replicates. Images are representative of at least $n=10$ imaged cells. Scale bars, 10 μm.

Article

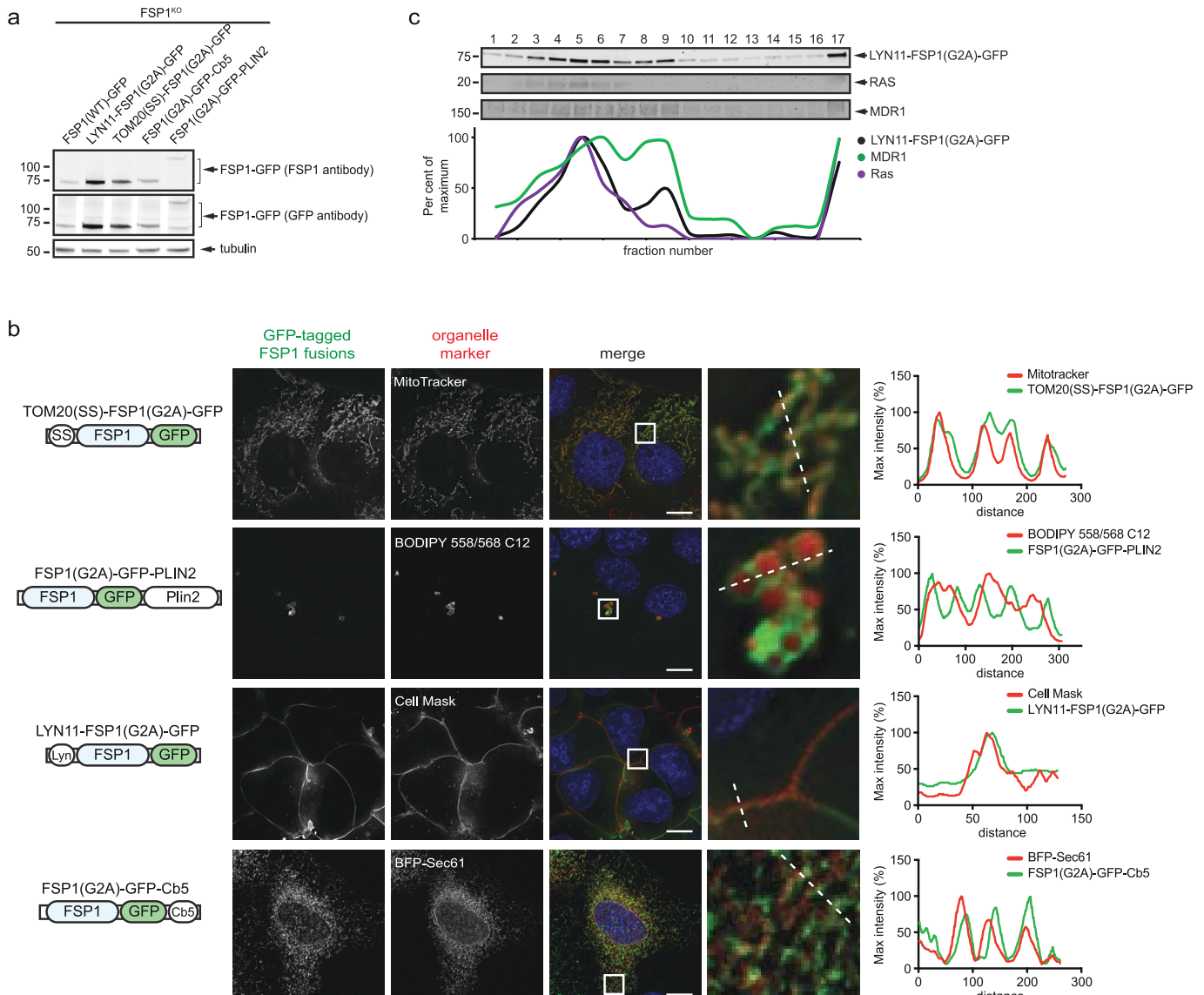


Extended Data Fig. 3 | Myristylation and lipid droplet localization of FSP1.

a, Schematic showing the procedure for metabolic labelling of cells with the myristate-alkyne YnMyr and conjugation of YnMyr-labelled proteins with TAMRA-azide-PEG-biotin using click chemistry. **b**, Analysis of FSP1 myristylation in buoyant fractions enriched in lipid droplets, by streptavidin enrichment of YnMyr-labelled proteins, click chemistry and SDS-PAGE. Cells were treated with 200 μ M oleate to induce lipid droplets and with 100 μ M YnMyr or 100 μ M myristate for 24 h. **c**, FSP1-GFP was induced with doxycycline for 24 h and cells were incubated with 100 μ M YnMyr for an additional 24 h to label proteins in the presence or absence of 75 μ M emetine. YnMyr-labelled

proteins were affinity-purified and analysed by click chemistry and SDS-PAGE.

d, Buoyant fractions enriched in lipid droplets, from cells expressing inducible FSP1-GFP, were isolated by sucrose gradient fractionation and analysed by western blot. Endo., endogenous FSP1. **e**, Inducible FSP1-GFP cells were treated with 200 μ M oleate in the presence or absence of 10 μ M NMT inhibitor, fixed and stained with anti-PLIN2 antibody before imaging. Images are representative of at least $n = 10$ imaged cells. Scale bar, 10 μ m. **f**, Western blot analysis of FSP1^{KO} cells induced for 48 h with doxycycline to express the indicated proteins. All panels are representative of two biological replicates.

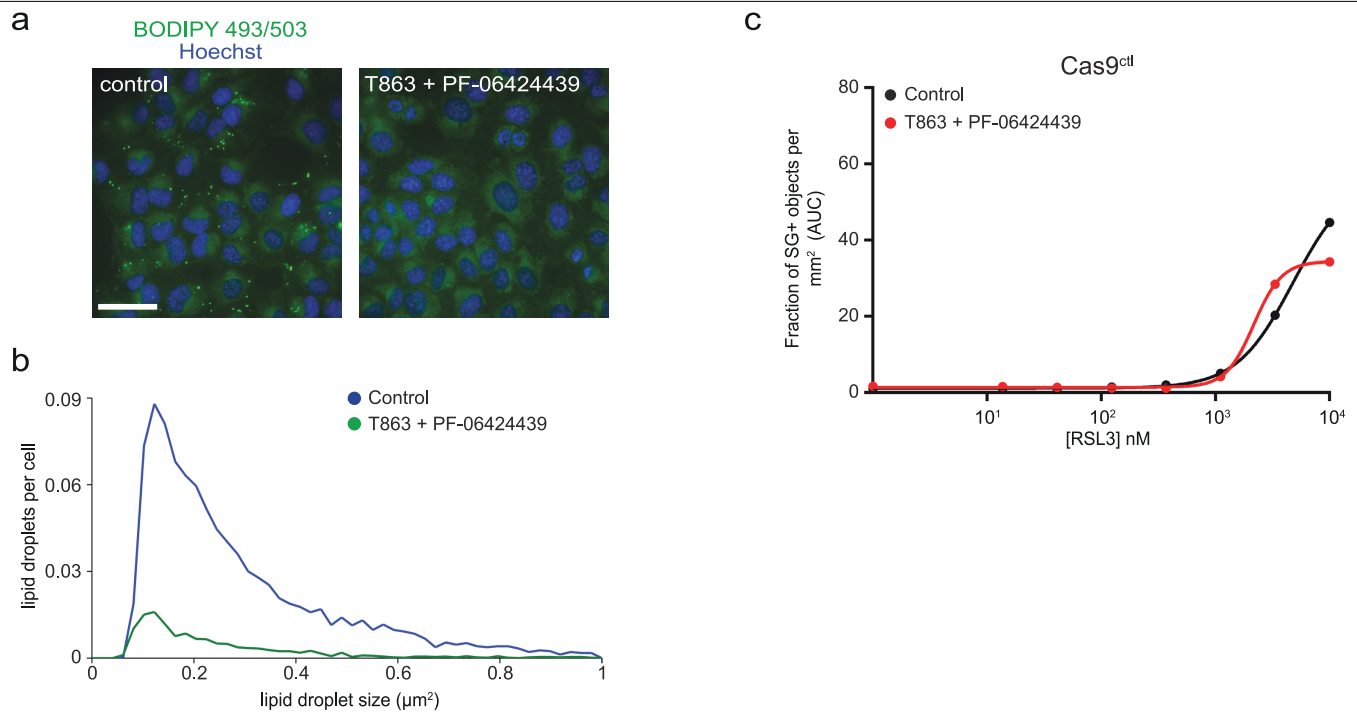


Extended Data Fig. 4 | Targeting of FSP1 to subcellular compartments.

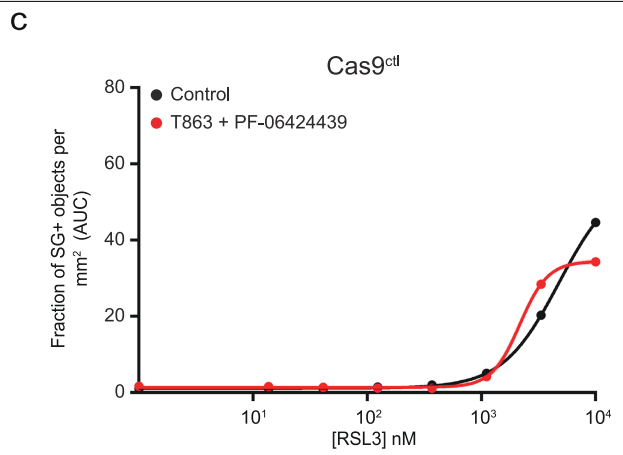
a, Western blot analysis of FSP1^{KO} cells induced for 48 h with doxycycline to express the indicated proteins. **b**, Live-cell microscopy of cells that express the indicated FSP1(G2A)-GFP constructs, incubated with 100 nM Mitotracker Orange to label mitochondria, 1 μM BODIPY 558/568 C12 to label lipid droplets or 5 μg ml⁻¹ Cell Mask to label the plasma membrane. To label the endoplasmic reticulum, cells were transiently transfected with BFP-Sec61 48 h before

imaging. Images are representative of at least $n=10$ imaged cells. Line intensity plots show colocalization between FSP1 and organelle markers. Scale bar, 10 μm. **c**, Plasma-membrane subdomains from FSP1^{KO} cells that express inducible LYN11-FSP1(G2A)-GFP were enriched by OptiPrep gradient centrifugation. The densitometry plot indicates the distribution of overexpressed and endogenous proteins. Panels are representative of two biological replicates except for **c**, which shows a single experiment.

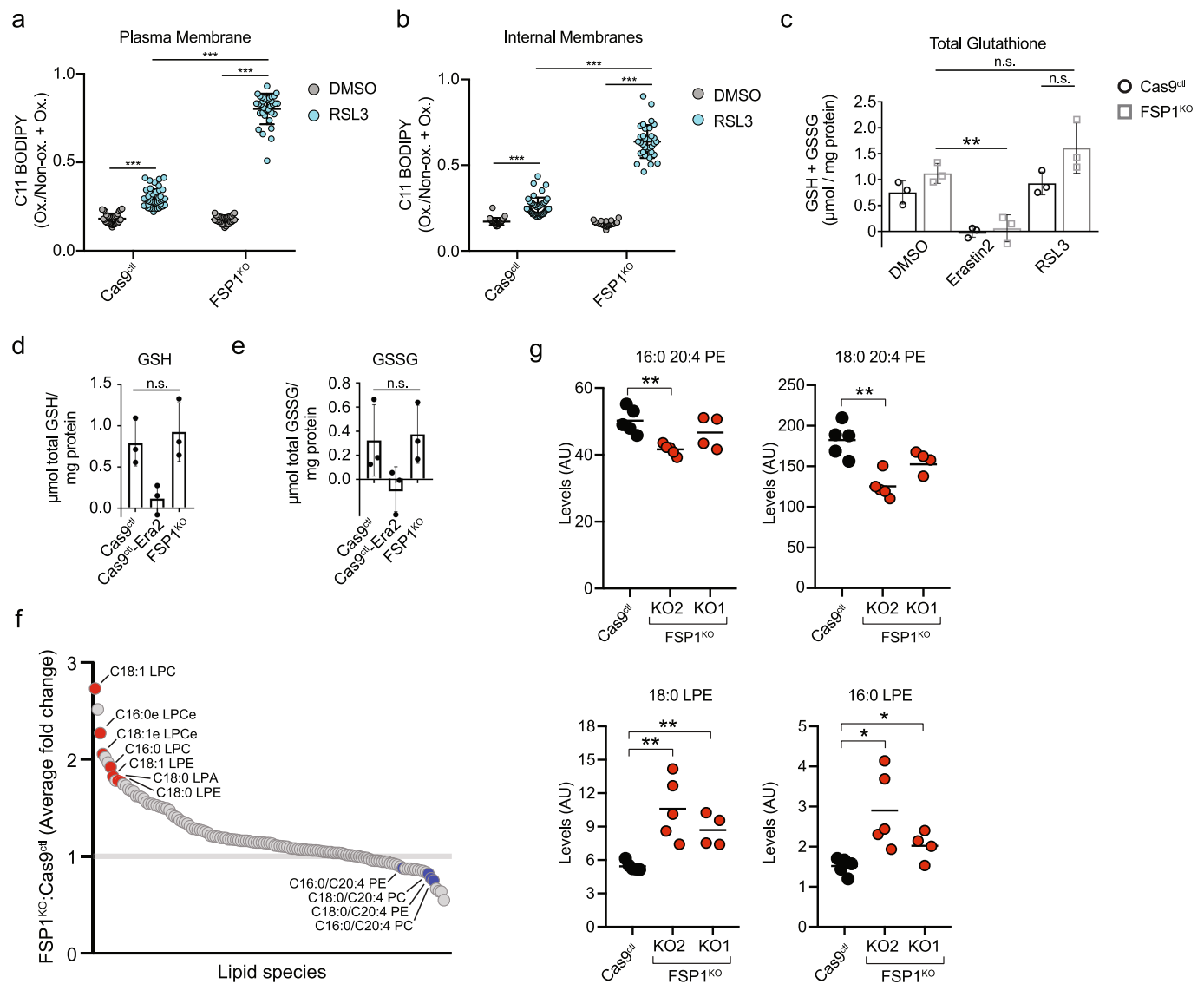
Article



Extended Data Fig. 5 | Lipid droplets are not required for inhibition of ferroptosis by FSP1. **a**, Control cells were treated with inhibitors of DGAT1 (20 μM T863) and DGAT2 (10 μM PF-06424439) for 48 h, stained with 1 μM BODIPY 493/503 and imaged by fluorescence microscopy. The image is representative of $n = 50$ imaged fields. Scale bar, 10 μm . **b**, The size and number



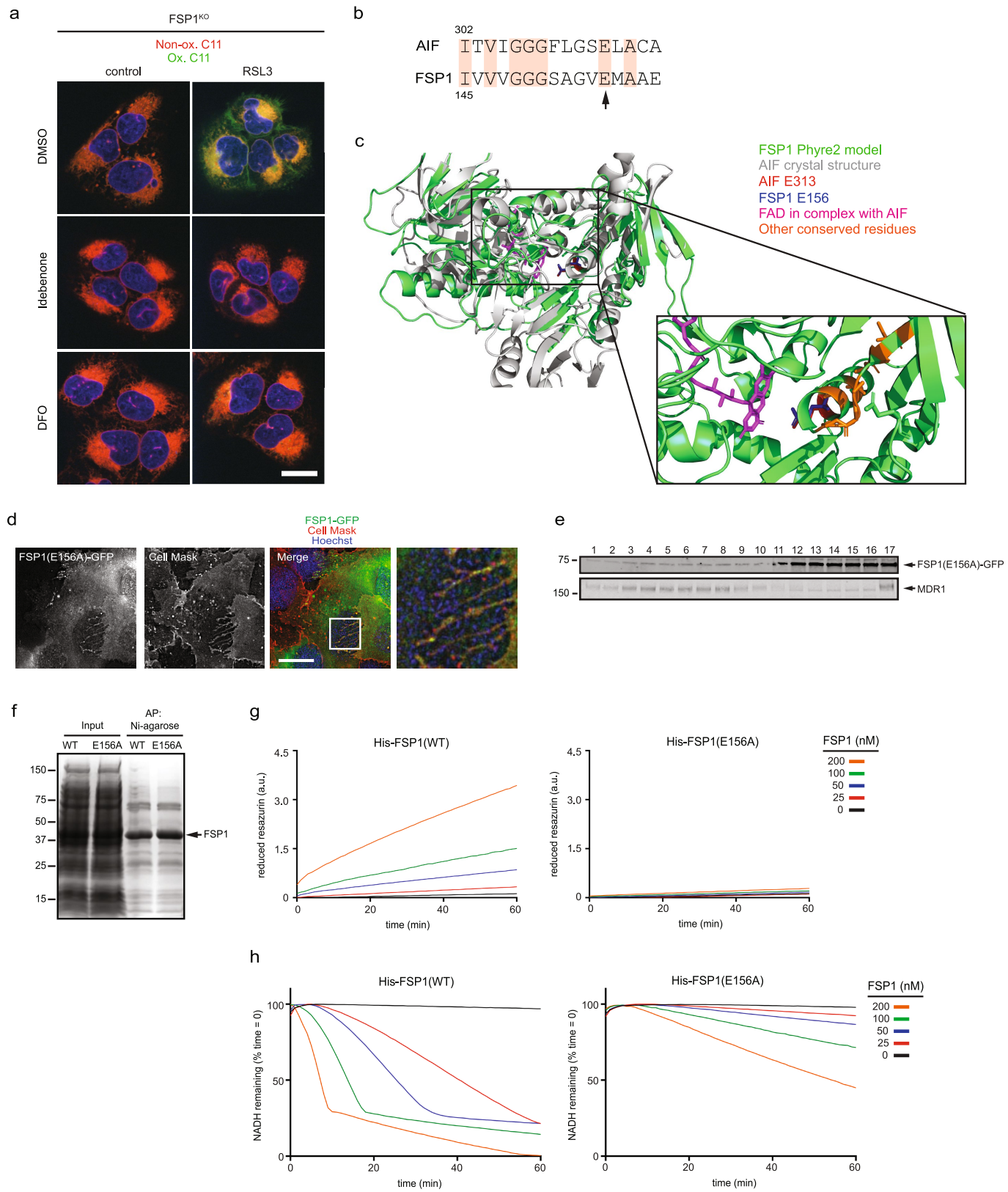
of lipid droplets were quantified from cells ($n > 5,000$) in **a,c**. Dose response of RSL3-induced cell death of control cells pretreated for 48 h with 20 μM T863 and 10 μM PF-06424439 before addition of RSL3. Each data point is the average of three technical replicates. All panels are representative of two biological replicates.



Extended Data Fig. 6 | Analysis of lipid peroxidation, glutathione and lipid levels in FSP1^{KO} cells. **a, b,** Ratio of oxidized-to-total BODIPY 581/591 C11 from images in Fig. 3a, at the plasma membrane (**a**) or at internal membranes (**b**). Each data point represents an individual cell quantified in one of two biological replicates. For **a**, Cas9^{ctrl} DMSO, $n=34$; Cas9^{ctrl} RSL3, $n=45$; FSP1^{KO} DMSO, $n=30$; FSP1^{KO} RSL3, $n=33$; *** $P<0.001$ by one-way ANOVA. For **b**, Cas9^{ctrl} DMSO, $n=33$; Cas9^{ctrl} RSL3, $n=45$; FSP1^{KO} DMSO, $n=30$; FSP1^{KO} RSL3, $n=33$; *** $P<0.001$ by one-way ANOVA. Error bars show mean \pm s.d. **c**, Total intracellular glutathione (GSH + GSSG) levels in control and FSP1^{KO} were determined following treatment with 250 nM RSL3 or 1 μ M Erastin2. The graph shows mean \pm s.d. of three biological replicates. n.s., FSP1^{KO} DMSO versus RSL3, $P=0.7278$; n.s., FSP1^{KO} RSL3 versus Cas9^{ctrl} RSL3, $P=0.1522$; ** $P=0.0072$ by one-way ANOVA.

d, e, GSH and GSSG levels in control and FSP1^{KO} cells were measured. Where indicated, cells were treated with 1 μ M Erastin2. The graph shows mean \pm s.d. of three biological replicates. n.s., GSH $P=0.6269$; n.s., GSSG $P=0.8284$ by two-tailed t -test. **f**, The plot shows the average of the fold change in lipids measured in two FSP1^{KO} cell lines generated using FSP1 sgRNA no. 1 and FSP1 sgRNA no. 2 (labelled KO1 and KO2, respectively), relative to control cells. Cas9^{ctrl}, $n=5$; KO1, $n=4$; KO2, $n=5$ biological replicates (Supplementary Table 3). **g**, Levels of select lipid species in biological replicates of control and FSP1^{KO} cells measured in **f**. The average values are indicated. 16:0 20:4 PE, ** $P=0.0017$; 18:0 20:4 PE, ** $P=0.0011$; 18:0 LPE, KO2 ** $P=0.0036$, KO1 ** $P=0.0019$; 16:0 LPE, KO2 * $P=0.0133$ and KO1 * $P=0.0335$ by two-tailed t -test.

Article

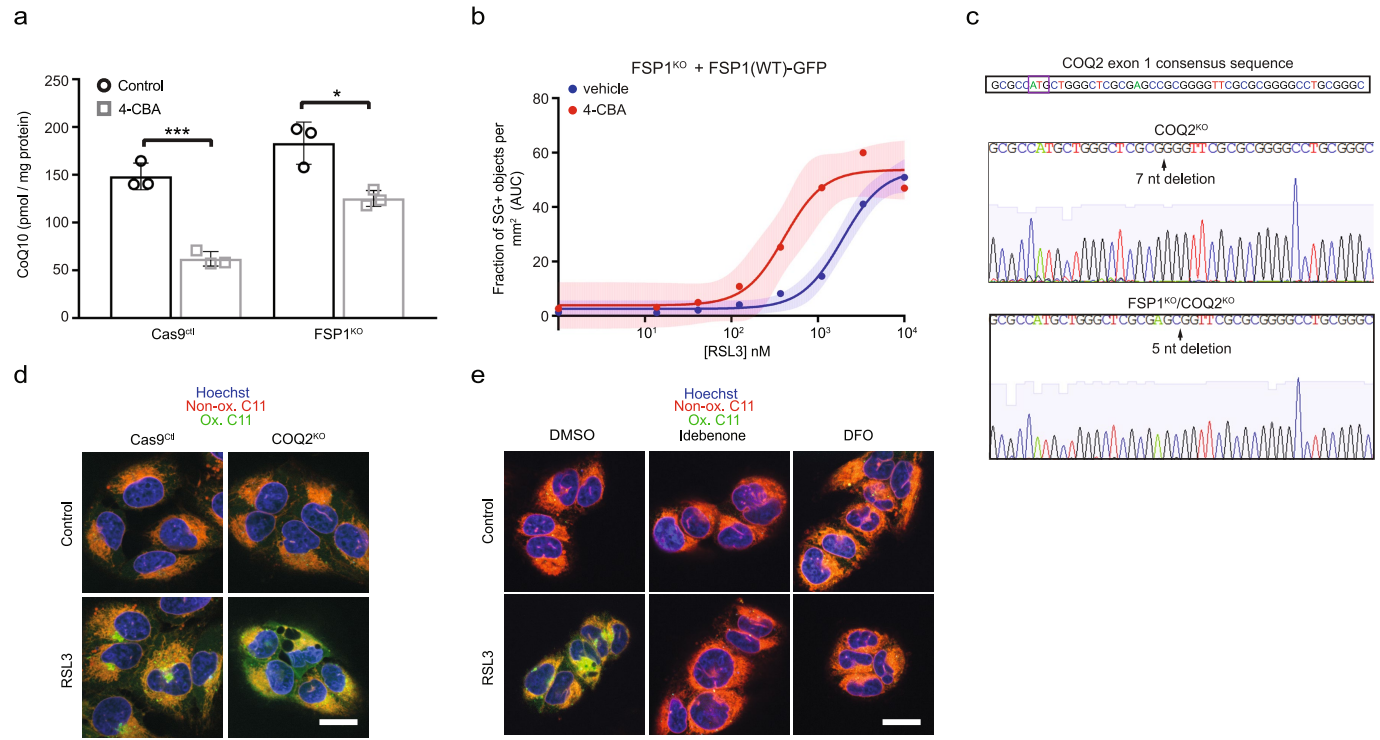


Extended Data Fig. 7 | See next page for caption.

Extended Data Fig. 7 | Analysis of the FSP1 oxidoreductase mutant. **a**, FSP1^{KO} cells were treated with 250 nM RSL3 and 10 µM idebenone or 50 µM DFO for 75 min, labelled with BODIPY 581/591 C11 and fixed before imaging. Images are representative of at least $n=10$ cells imaged for each treatment condition. Scale bar, 20 µm. **b**, Sequence alignment showing residues conserved between AIF and FSP1. The arrow points to E313 in AIF (aligns to E156 in FSP1) that functions in binding to flavin adenine dinucleotide. **c**, Structural alignment between the crystal structure of mouse AIF (RCSB Protein Data Bank code (PDB) 1GV4) and the Phyre2-generated model of FSP1. **d**, Live-cell microscopy of

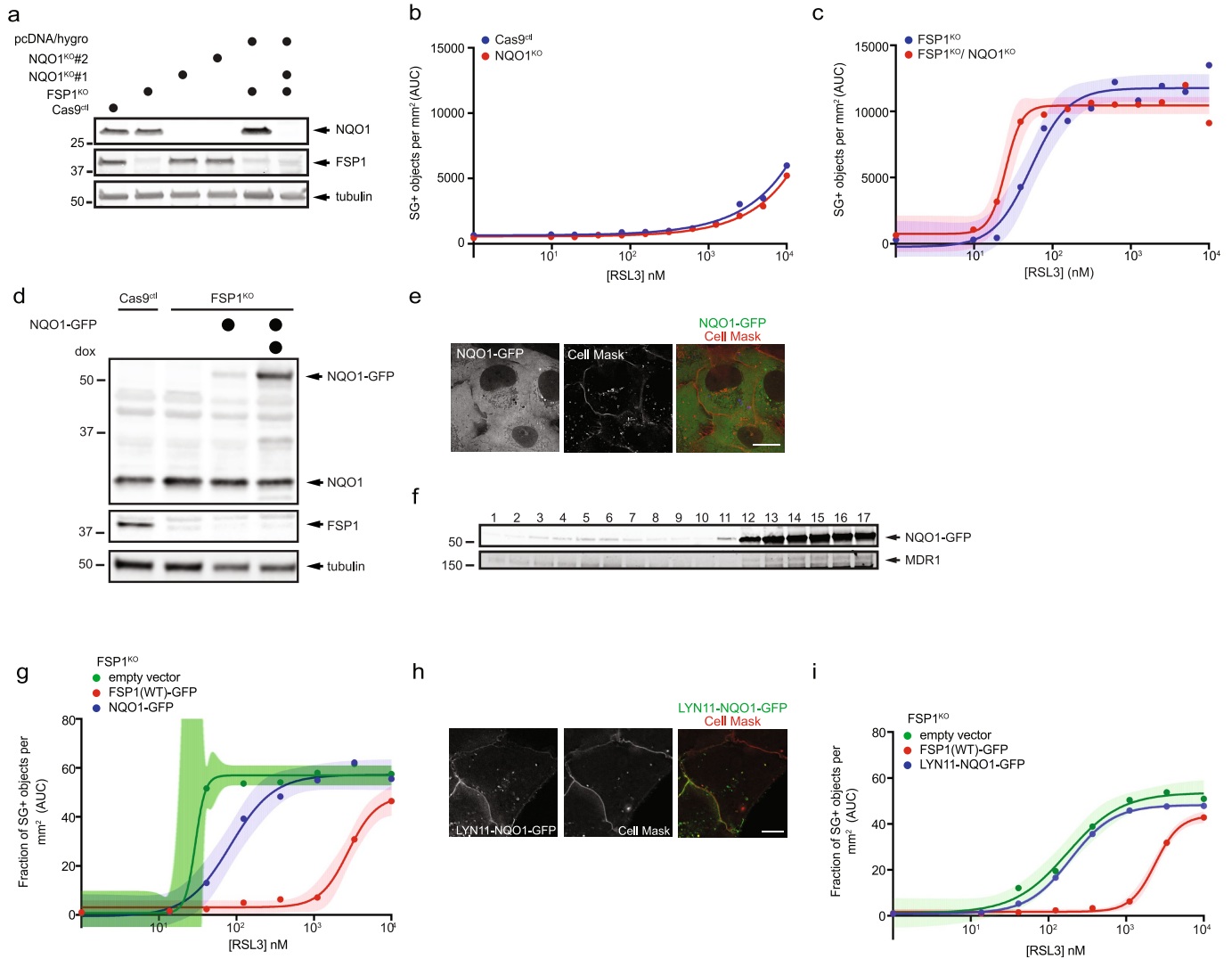
FSP1^{KO} cells expressing inducible FSP1(E156A)-GFP labelled with 5 µg ml⁻¹ Cell Mask. The image is representative of at least $n=10$ imaged cells. Scale bar, 10 µm. **e**, Plasma-membrane subdomains from FSP1^{KO} cells that express FSP1(E156A)-GFP were enriched by OptiPrep gradient centrifugation. **f**, SDS-PAGE and Coomassie brilliant blue stain of recombinant His-FSP1(WT) and His-FSP1(E156A) purified with Ni-NTA agarose beads. **g**, Reduction of resazurin by recombinant FSP1 in the presence of NADH. **h**, Oxidation of NADH by recombinant FSP1 in the presence of coenzyme Q₁. Panels **g** and **h** are representative of two biological replicates, and **e** shows a single experiment.

Article



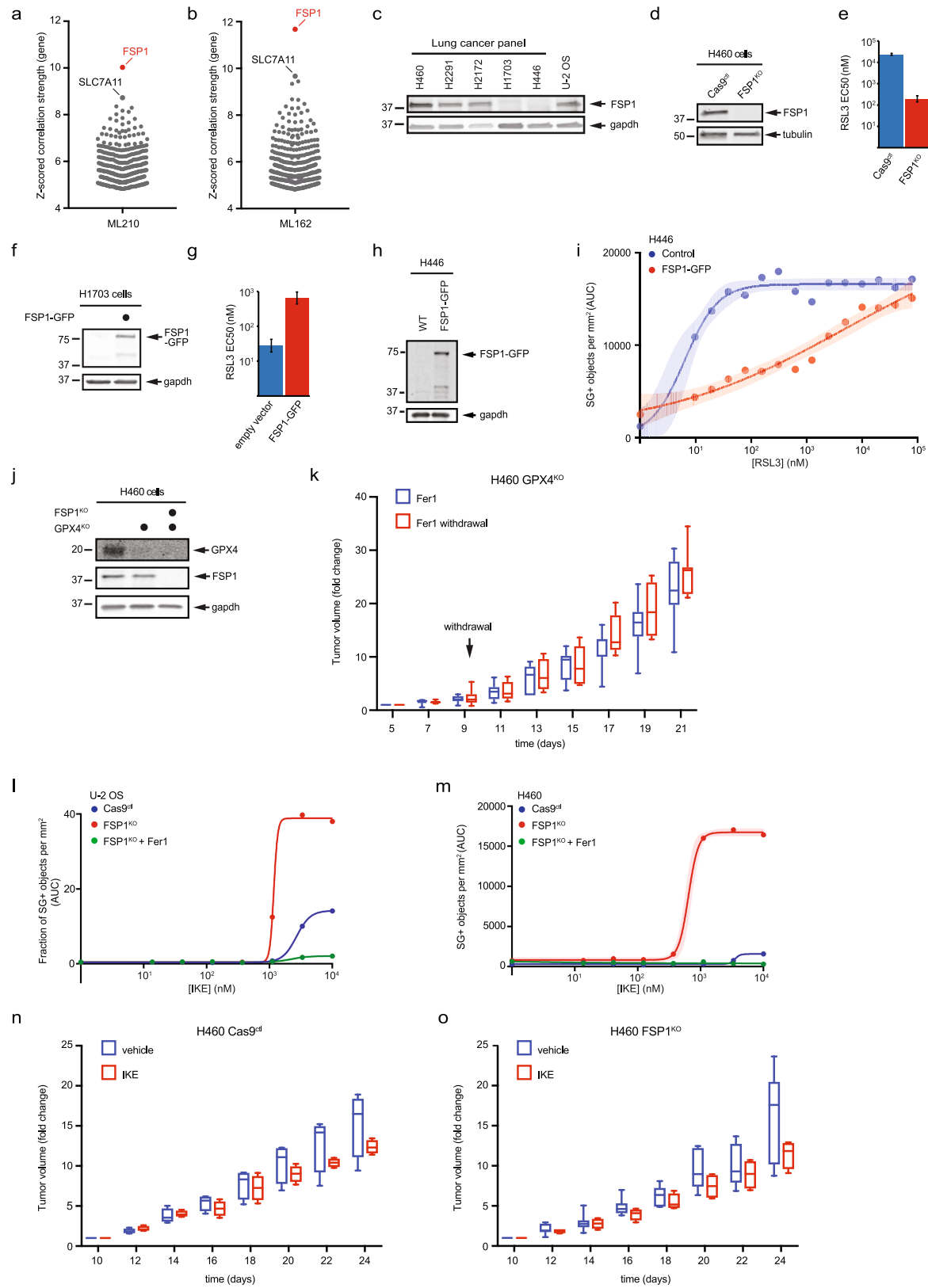
Extended Data Fig. 8 | Lipid peroxidation in CoQ-depleted cells. **a**, Total CoQ levels in control and FSP1^{KO} cells treated for 48 h with 3 mM 4-CBA. The graph shows mean \pm s.d. of three biological replicates. *** P =0.0007, * P =0.0132 by two-tailed *t*-test. **b**, Dose response of RSL3-induced death of inducible FSP1-GFP cells pretreated for 48 h with 3 mM 4-CBA and doxycycline before addition of RSL3. Shading indicates 95% confidence intervals for the fitted curves and each data point is the average of three technical replicates. The panel is representative of two biological replicates. **c**, Genomic sequencing of the

COQ2 gene in COQ2^{KO} and FSP1^{KO} COQ2^{KO} cells. The ATG start codon is boxed in the COQ2 consensus sequence. **d**, Control and COQ2^{KO} cells treated with 250 nM RSL3 for 3 h were labelled with BODIPY 581/591 C11 and fixed before imaging. **e**, COQ2^{KO} cells were treated with 250 nM RSL3 and 10 μ M idebenone or 50 μ M DFO for 3 h, labelled with BODIPY 581/591 C11 and fixed before imaging. In panels **d**, **e**, images are representative of at least n =10 cells imaged for each treatment condition. Scale bars, 20 μ m.



Extended Data Fig. 9 | Role of NQO1 in ferroptosis resistance. **a**, Western blot analysis of lysates from NQO1^{KO} and NQO1^{KO} FSP1^{KO} cells. **b**, Dose response of RSL3-induced death of control and NQO1^{KO} cells. **c**, Dose response of RSL3-induced death of FSP1^{KO} and NQO1^{KO} FSP1^{KO} cells. Cells in **b** and **c** were generated using *NQO1* sgRNA 1. **d**, Western blot analysis of lysates of FSP1^{KO} cells that express doxycycline-inducible NQO1-GFP. **e**, Live-cell microscopy of inducible NQO1-GFP cells labelled with 5 µg ml⁻¹ Cell Mask. **f**, Plasma-membrane subdomains from FSP1^{KO} cells that express NQO1-GFP were enriched by OptiPrep gradient centrifugation. **g**, Dose response of RSL3-induced death of

FSP1^{KO} cells expressing the indicated inducible constructs. **h**, Live-cell microscopy of FSP1^{KO} cells that express inducible LYN11-NQO1-GFP labelled with 5 µg ml⁻¹ Cell Mask. **i**, Dose response of RSL3-induced death of FSP1^{KO} cells that express the indicated inducible constructs. For panels **b**, **c**, **g**, **i**, shading indicates 95% confidence intervals for the fitted curves and each data point is the average of three technical replicates. Panels are representative of two biological replicates except for **f** and **i**, which show the results of single experiments. In **e** and **h**, the images are representative of at least $n=10$ imaged cells. Scale bars, 10 µm.



Extended Data Fig. 10 | See next page for caption.

Extended Data Fig. 10 | The role of FSP1 in cancer. **a, b**, A high level of expression of FSP1 is correlated with resistance to the GPX4 inhibitors ML210 (**a**) and ML162 (**b**) in non-haematopoietic cancer cells. Plotted data were mined from the CTRP database that contains correlation coefficients between gene expression and drug sensitivity for 907 cancer cell lines treated with 545 compounds. Plotted values are z-scored Pearson's correlation coefficients. **c**, Western blot of FSP1 expression in a panel of lung cancer lines. **d**, Western blot of lysates from control and FSP1^{KO} H460 cells. **e**, EC₅₀ RSL3 dose for the indicated H460 cell lines was calculated from the results in Fig. 1d. Bars indicate 95% confidence intervals. **f**, Western blot of lysates from control and H1703 cells. **g**, EC₅₀ RSL3 dose for the indicated H1703 cell lines was calculated from the results in Fig. 1e. Bars indicate 95% confidence intervals. **h**, Western blot analysis of H446 cells that express doxycycline-inducible FSP1-GFP. **i**, Dose response of RSL3-induced death of control and FSP1-GFP H446 cells. **j**, Western blot analysis of GPX4^{KO} and GPX4^{KO} FSP1^{KO} H460 cells. **k**, GPX4^{KO} H460 tumour xenograft cells were initiated in immune-deficient SCID mice ($n=16$). Following 5 days of daily Fer1 injections (2 mg kg⁻¹ body weight) to allow lines to

develop tumours, 1 set of mice ($n=8$) continued to receive daily Fer1 injections and a second set ($n=8$) received vehicle injections for the remaining 17 days. The distribution of fold changes in sizes of individual tumours during the treatment is shown. GPX4^{KO} (−) Fer1, $n=7$; GPX4^{KO} (+) Fer1, $n=7$. **l**, Dose response of IKE-induced death of control and FSP1^{KO} U-2 OS cells. **m**, Dose response of IKE-induced death of control and FSP1^{KO} H460 cells. **n, o**, Control (**n**) and FSP1^{KO} (**o**) H460 tumour xenografts were initiated in immune-deficient SCID mice ($n=16$). After 10 days, each group of mice ($n=8$) was injected daily with IKE or vehicle (40 mg kg⁻¹ body weight). The distribution of fold changes in sizes of individual tumours during the treatment is shown. Cas9^{ctd} (−) IKE, $n=4$; Cas9^{ctd} (+) IKE, $n=4$; FSP1^{KO} (−) IKE, $n=7$; FSP1^{KO} (+) IKE, $n=4$. In **k, n, o**, box plots show median, 25th and 75th percentiles, minima and maxima of the distributions. Panels are representative of two biological replicates except **l, m**, which show the results of single experiments. In **i, l, m**, shading indicates 95% confidence intervals for the fitted curves and each data point is the average of three technical replicates.

Corresponding author(s): James Olzmann

Last updated by author(s): Sep 5, 2019

Reporting Summary

Nature Research wishes to improve the reproducibility of the work that we publish. This form provides structure for consistency and transparency in reporting. For further information on Nature Research policies, see [Authors & Referees](#) and the [Editorial Policy Checklist](#).

Statistics

For all statistical analyses, confirm that the following items are present in the figure legend, table legend, main text, or Methods section.

n/a Confirmed

- The exact sample size (n) for each experimental group/condition, given as a discrete number and unit of measurement
- A statement on whether measurements were taken from distinct samples or whether the same sample was measured repeatedly
- The statistical test(s) used AND whether they are one- or two-sided
Only common tests should be described solely by name; describe more complex techniques in the Methods section.
- A description of all covariates tested
- A description of any assumptions or corrections, such as tests of normality and adjustment for multiple comparisons
- A full description of the statistical parameters including central tendency (e.g. means) or other basic estimates (e.g. regression coefficient) AND variation (e.g. standard deviation) or associated estimates of uncertainty (e.g. confidence intervals)
- For null hypothesis testing, the test statistic (e.g. F , t , r) with confidence intervals, effect sizes, degrees of freedom and P value noted
Give P values as exact values whenever suitable.
- For Bayesian analysis, information on the choice of priors and Markov chain Monte Carlo settings
- For hierarchical and complex designs, identification of the appropriate level for tests and full reporting of outcomes
- Estimates of effect sizes (e.g. Cohen's d , Pearson's r), indicating how they were calculated

Our web collection on [statistics for biologists](#) contains articles on many of the points above.

Software and code

Policy information about [availability of computer code](#)

Data collection

SoftWoRx V6.5.2 (GE Life Sciences), PHYRE2 Protein Fold Recognition Software V2.0 (www.sbg.bio.ac.uk/phyre2), BD FACSDiva V6.2 (bdbiosciences.com), SoftMax Pro V6.3 (moleculardevices.com), iQ3 live cell imaging software (Andor Technology), EZChrom Elite V3.2.0 (Agilent), Image Lab V6.0.1 (Bio-Rad Laboratories, Inc.)

Data analysis

casTLE statistical framework V1.0 (bitbucket.org/dmorgens/castle), ImageJ V1.8.0 (imagej.nih.gov/ij), MATLAB R2016b (mathworks.com), droplet detection and quantification software for MATLAB (Olzmann lab, www.dropletproteome.org), Prism V7 (GraphPad), Zoom Image Analysis Software 2016B (Essen Bioscience), BowTie 2 V2.3.4.3 (bowtie-bio.sourceforge.net/bowtie2/index.shtml), FlowJo V10 (TreeStar) (flowjo.com)

For manuscripts utilizing custom algorithms or software that are central to the research but not yet described in published literature, software must be made available to editors/reviewers. We strongly encourage code deposition in a community repository (e.g. GitHub). See the Nature Research [guidelines for submitting code & software](#) for further information.

Data

Policy information about [availability of data](#)

All manuscripts must include a [data availability statement](#). This statement should provide the following information, where applicable:

- Accession codes, unique identifiers, or web links for publicly available datasets
- A list of figures that have associated raw data
- A description of any restrictions on data availability

All data that support the conclusions in this manuscript are available from the corresponding author upon request. Raw data for figure 1 can be accessed in Supplementary Table 1. Raw data for figure 3 can be accessed in Supplementary Table 3. Raw data for figure 4 can be accessed in Supplementary Table 4 and are publicly available from the CTRP and CCLE databases (portals.broadinstitute.org).

Field-specific reporting

Please select the one below that is the best fit for your research. If you are not sure, read the appropriate sections before making your selection.

Life sciences Behavioural & social sciences Ecological, evolutionary & environmental sciences

For a reference copy of the document with all sections, see nature.com/documents/nr-reporting-summary-flat.pdf

Life sciences study design

All studies must disclose on these points even when the disclosure is negative.

Sample size	No statistical tests were used to calculate sample size. In cases where statistics were derived, sample size was n=3 or more independent biological replicates. For measurement of lipid levels using mass spectrometry and measurement of reduced COQ levels using HPLC, sample sizes were n=5 and n=6 biological replicates, respectively, to account for expected variability due to sample preparation and noise from the instruments. For mouse xenograft experiments, sample size was n=8 for each treatment group to account for differences in tumor formation and growth, and to ensure recovery of a sufficient quantity of mice with successful xenografts of approved size at each time point of the study.
Data exclusions	These criteria were established prior to performing the xenograft studies. In the ferrostatin-1 withdrawal experiments, animals not included in the analysis included mice that were sacrificed early due to sickness (n = 1 of GPX4KO (+) Fer1) and mice whose tumors were determined to be outliers according to the Grubbs statistical test using Prism (Graphpad) software (n = 1 of GPX4KO (-) Fer1 and n = 1 of GPX4KO/FSP1KO (-) Fer1). For the IKE injection experiments, animals not included in the analysis included mice that were sacrificed early due to development of exceedingly large tumors (n = 1 of Cas9 ctrl (+) IKE, n = 3 of Cas9 ctrl (-) IKE, n = 3 of FSP1KO (+) IKE and n = 1 of FSP1KO (-) IKE), mice in which tumors failed to initiate (n = 2 of Cas9 ctrl (+) IKE), and mice whose tumors were determined to be statistical outliers according to the Grubbs test (n = 1 of Cas9 ctrl (+) IKE, n = 1 of Cas9 ctrl (-) IKE, n = 1 of FSP1KO (+) IKE).
Replication	All attempts at replication were successful. Figures, including western blots, dose response curves and enzymatic activity assay panels are representative of two biological replicates except for the following, which show single experiments: plasma membrane fractionations in Extended Data Fig. 4c, 7e and 9f and cell death curves in Extended Data Fig. 1d,e, 1k,j, 9i and 10l,m. Images are representative of at least n = 10 imaged cells.
Randomization	For the xenograft studies, following injection of H460 cells, the mice were randomly assigned into 2 treatment groups for the ferrostatin-1 withdrawal experiments and into 2 treatment groups for the IKE injection experiments.
Blinding	Blinding was not possible because the experiments were performed by a single researcher.

Reporting for specific materials, systems and methods

We require information from authors about some types of materials, experimental systems and methods used in many studies. Here, indicate whether each material, system or method listed is relevant to your study. If you are not sure if a list item applies to your research, read the appropriate section before selecting a response.

Materials & experimental systems

n/a	Involved in the study
<input type="checkbox"/>	<input checked="" type="checkbox"/> Antibodies
<input type="checkbox"/>	<input checked="" type="checkbox"/> Eukaryotic cell lines
<input checked="" type="checkbox"/>	<input type="checkbox"/> Palaeontology
<input type="checkbox"/>	<input checked="" type="checkbox"/> Animals and other organisms
<input checked="" type="checkbox"/>	<input type="checkbox"/> Human research participants
<input checked="" type="checkbox"/>	<input type="checkbox"/> Clinical data

Methods

n/a	Involved in the study
<input checked="" type="checkbox"/>	<input type="checkbox"/> ChIP-seq
<input type="checkbox"/>	<input checked="" type="checkbox"/> Flow cytometry
<input checked="" type="checkbox"/>	<input type="checkbox"/> MRI-based neuroimaging

Antibodies

Antibodies used

Anti-Plin2 (Abgent, cat. #AP5118c), anti-AIFM2 (Proteintech Group, Inc. cat. #20886-1-AP and Santa Cruz Biotechnology, clone B-6, cat. #sc-377120), anti- α -tubulin (Cell Signaling Technology, Inc., cat. #2144 and Santa Cruz Biotechnology, clone B-7, cat. #sc-5286), anti-GPX4 (Abcam, cat. #ab41787), anti-ACSL4 (Sigma-Aldrich, cat. #SAB-2701949), anti-GFP (Poteintech Group, Inc., clone 1E10H7, cat. #66002-1-1), anti-NQO1 (Proteintech Group, Inc., cat. #1145-1-AP), anti-GAPDH (EMD Millipore, cat. #mab374), anti-RAS (Cell Biolabs, Inc. cat. #STA-400), anti-MDR1 (Cell Signaling Technology, Inc., clone D3H1Q, cat. #12683S), anti-p21 (Cell Signaling Technology, Inc., clone 12D1, cat. #2947).

Validation

Anti-AIFM2, anti-GPX4, anti-ACSL4, and anti-NQO1 were validated using genetic knockout of the endogenous genes with Cas9 and one or more targeted sgRNAs. Anti-Plin2, anti- α -tubulin, anti-GAPDH, anti-RAS, anti-MDR1 and anti-p21 were validated in human cells by the manufacturer.

Eukaryotic cell lines

Policy information about [cell lines](#)

Cell line source(s)	H460, H2291, H2172, H1703, H446 were purchased from ATCC (atcc.org). U-2 OS Flp-In cells were a gift from Dr. Daniel Durocher (Lunenfeld-Tenenbaum Research Institute).
Authentication	None of the cell lines used were authenticated.
Mycoplasma contamination	All cell lines are negative for mycoplasma contamination.
Commonly misidentified lines (See ICLAC register)	Cell lines used in the study are not flagged in the Register of Misidentified Cell Lines.

Animals and other organisms

Policy information about [studies involving animals; ARRIVE guidelines](#) recommended for reporting animal research

Laboratory animals	Male, C.B17 SCID mice, 6 weeks of age
Wild animals	The study did not involve wild animals.
Field-collected samples	The study did not involve field-collected samples.
Ethics oversight	All animal experiments were conducted in accordance with the guidelines of the Institutional Animal Care and Use Committees (IACUC) of the University of California, Berkeley.

Note that full information on the approval of the study protocol must also be provided in the manuscript.

Flow Cytometry

Plots

Confirm that:

- The axis labels state the marker and fluorochrome used (e.g. CD4-FITC).
- The axis scales are clearly visible. Include numbers along axes only for bottom left plot of group (a 'group' is an analysis of identical markers).
- All plots are contour plots with outliers or pseudocolor plots.
- A numerical value for number of cells or percentage (with statistics) is provided.

Methodology

Sample preparation	Cells grown in 6-cm plates were washed with PBS, trypsinized and centrifuged for 5 min at 500 × g. Cell pellets were resuspended in PBS containing 5% FBS and 5 µM CellEvent™ Caspase-3/7 Green Detection Reagent, and were incubated for 30 min at 37°C prior to analysis.
Instrument	LSRFortessa (Becton-Dickinson)
Software	Data was collected using BD FACSDiva V6.2 (Becton-Dickinson) and analyzed using FlowJo V10 (TreeStar).
Cell population abundance	Cells were not sorted during the procedure.

Gating strategy
Apoptotic cells were gated using the same low FSC threshold (FSC- gate) across all samples and the FITC signals of the gated populations were determined.

- Tick this box to confirm that a figure exemplifying the gating strategy is provided in the Supplementary Information.